April 28, 2023

Phylogenomic time tree of bryophytes resolves 500 million years of diversification

Author list:

Julia Bechteler[1] *, Gabriel Peñaloza-Bojacá[2]*, David Bell[3], Gordon Burleigh[4]*, Stuart McDaniel[4], Christine Davis[4], Emily Sessa[4 5], Alexander Bippus[6], D. Christine Cargill[7], Sahut Chantanoarrapint[8], Isabel Draper[9], Lorena Endara[4, 10], Laura L. Forrest[3], Ricardo Garilleti[11], Sean W. Graham[12], Sanna Huttunen[13], Javier Jauregui Lazo[14], Francisco Lara[9], Juan Larraín[15], Lily Lewis[4], David Long[3], Dietmar Quandt[1], Karen Renzaglia[16], Alfons Schäfer-Verwimp[17], Gaik Ee Lee[18] Adriel Sierra Pinilla[19], Matt von Konrat[20], Charles Zartman[21], Bernard Goffinet [22] *& Juan Carlos Villarreal A. [19] *

[1]Nees-Institute for Plant Biodiversity, University of Bonn, Meckenheimer Allee 170, 53115 Bonn, Germany. [2]Laboratório de Sistemática Vegetal, Departamento de Botânica, Instituto de Ciências Biológicas, Universidade Federal de Minas Gerais. [3]Royal Botanic Garden Edinburgh, 20A Inverleith Row, Edinburgh EH3 5LR, United Kingdom. [4]Department of Biological Sciences, 220 Bartram Hall, University of Florida, Gainesville, FL 32611, USA. [5] Present address: The New York Botanical Garden, 2900 Southern Boulevard, Bronx, NY, 10458, USA. [6]California State Polytechnic University, Humboldt, Arcata, CA 95521. [7]Australian National Herbarium, Centre for Australian National Biodiversity Research, GPO Box 1700, Canberra. ACT. 2601. [8]PSU Herbarium, Division of Biological Science, Faculty of Science Prince of Songkla University, Hat Yai, Songkhla, 90110, Thailand. [9]

Departamento de Biología, Facultad de Ciencias, Universidad Autónoma de Madrid, 28049 Madrid, Spain / Centro de Investigación en Biodiversidad y Cambio Global, Universidad Autónoma de Madrid, Madrid, Spain. [10] Present address: Department of Biological Sciences, 132 Long Hall, Clemson University, Clemson, SC 29634, USA. [11]Departamento de Botánica y Geología. Universidad de Valencia, Avda. Vicente Andrés Estelles s/n, 46100 Burjassot, Spain. [12]Department of Botany, University of British Columbia, 6270 University Boulevard, Vancouver, British Columbia, V6T 1Z4, Canada. [13]Herbarium (TUR), Biodiversity Unit, 20014 University of Turku, Finland. [14]Department of Plant Biology and Genome Center, University of California Davis, 451 Health Sciences Drive, Davis, 95616, USA. [15]Centro de Investigación en Recursos Naturales y Sustentabilidad (CIRENYS), Universidad Bernardo O'Higgins, Avenida Viel 1497, Santiago, Chile. [16]Southern Illinois University, IL 62901, Carbondale, USA. [17]Mittlere Letten 11, 88634 Herdwangen-Schönach, Germany. [18] Faculty of Science and Marine Environment/Institute of Tropical Biodiversity and Sustainable Development, Universiti Malaysia Terengganu, 21020 Kuala Nerus, Terengganu, Malaysia. [19]Department de Biologie, Université Laval, Québec, QC, Canada. [20]Gantz Family Collections Center, Field Museum, 1400 S. DuSable Lake Shore Drive, Chicago, IL 60605, U.S.A. [21] Instituto Nacional de Pesquisas da Amazônia, Departamento de Biodiversidade, Avenida André Araújo, 2936, Aleixo, CEP 69060-001, Manaus, AM (Brazil) f [22]Ecology and Evolutionary Biology, 75 NorthEagleville road, University of Connecticut, Storrs CT, 06269-3043, USA.

Abstract – 200 words

Bryophytes are emerging as the sister-group to extant vascular plants, and their current diversity highlights that their life cycle characterized by a dominating vegetative gametophyte and an unbranched sporophyte composes a successful alternative to that of vascular plants and their dominating sporophyte. The evolutionary history of hornworts, liverworts and mosses remains, however, poorly resolved, due in part to the small character space from which to draw shared ancestry. Our understanding of the diversification of these lineages has been significantly reshaped by inferences from molecular data, highlighting extensive homoplasy in various traits and repeated bursts of diversification. Here, we present the first bryophyte time-tree based on 228 nuclear genes sampled via target capture for 531 species with divergence times estimated based on a comprehensive set of fossil calibrations. Our phylogenetic trees reflect a robust backbone, highlight novel ordinal relationships and circumscriptions, and the recognition of 13 new orders of liverworts and mosses. Our time-tree reveals that most orders originated prior to the Cretaceous, confirms the Cretaceous radiation of the hyperdiverse hypnalean mosses and species-rich liverwort clades. This comprehensive resource provides a robust and expandable phylogenomic framework for evolutionary analyses across lineages in this diverse and important group of land plants.

Keywords: Community resource, Cretaceous diversification, Hornworts, Land plants, Liverworts, Mosses, Phylogenomic, Rapid diversification.

Introduction

The emerging consensus that bryophytes, which comprise hornworts, liverworts, and mosses (Fig. 1), form the sister group to extant vascular plants[1,2] raises important questions about the morphology and life cycle of the first land plants[3]. Key elements of land plant development, including meristem function[4], stomatal development[5], and hormone responses[6,7], are built from a conserved genomic blueprint[5], and bryophytes hold signatures of divergence and reduction from an ancestor with at least a morphologically more complex sporophyte[8]. Bryophytes are important components of various ecological communities and contribute to local nutrients fluxes and global biogeochemical cycles[9–11]. Broad evolutionary analyses are key for assessing the significance of vegetative gametophyte trait in these roles. Reconstructing the history of bryophytes and hence of character transformations are therefore critical for understanding the transformations of developmental, physiological and functional morphological traits across land plants[1,8,12].

Unraveling the relationships and time of divergence among major lineages of bryophytes has been hampered by the putative low morphological character space, the high homoplasy in the evolution of these traits, the shortage of phylogenetically informative ontogenetic data, the paucity of fossil taxa and the difficulty in reliably assigning these to lineages defined by extant taxa. Furthermore, phylogenetic inferences suffer from insufficient signal, especially across major lineages, due perhaps to their old divergence, and hence substitutional saturation or their rapid diversification. All prior reconstructions rely on either a few loci sampled for perhaps many species, or many markers sampled for a few bryophyte taxa[8,13–16].

We present the first comprehensive phylogeny of bryophytes based on 228 markers sampled for 531 species from across all orders, using the GoFlag 408 probe set. We then calibrated this phylogeny based on the most recent assessments of the affinities of liverwort[17] and moss[18] fossils to estimate divergence times. We acquired homologous sequences for virtually all samples and recovered strong support for many relationships between classes and orders. We confirm the persisting phylogenetic ambiguity for others and propose three new liverwort and ten new moss orders. As in vascular plants, significant conflict among genes both within rapidly diversifying groups of bryophytes and among the oldest nodes is likely due to incomplete lineage sorting, ancient hybridization, and lack of signal in explosive radiations. We have unraveled the macroevolutionary history of this key group of land plants using the GoFlag 408 probe set, which emerged as a powerful tool to tackle the complexity of the diversification process at multiple phylogenetic scales across the bryophytes[19].

Results and Discussion

We sampled 533 samples representing 531 species from 499 genera distributed among 72% of families from all 69 orders of bryophytes (Figs 1–3; Extended Data Figs. 1–7; Supplementary Figs. S1–S9; Supplementary Tables S1–S11). The alignment of sequences from 228 targeted nuclear genes varies in length, variable sites, potentially parsimony informative sites and GC content (Supplementary Table S4). The average alignment length was 339.74 bp (min=120, max=1459) with most

(n=146) over 200 bp long. Parsimony informative sites were correlated with alignment length (R^2 = 0.9593) with a mean of 238.42 sites per alignment (min=66, max=1065) and a low percentage of missing data (8.61%, SD=0.43).

Coalescent-based (ASTRAL) and maximum likelihood (ML) concatenated super-matrix analyses (IQ-TREE) of nucleotide and amino-acid data yielded similar results (Extended Data Figs. 1-7). In the following sections, we present the results from the ASTRAL analyses of nucleotide and amino-acid data including quartet values and gene concordance factors (gCF) and site concordance factors (sCF). We refer to a majority of gene trees when more than 50% of these share a given signal, and a plurality of gene trees when the proportion of trees supporting the topology is higher than 33% but less than 50%. The gene concordance factor (gCF) and site concordance factor (sCF) represent the percentage of decisive gene trees and sites containing a specific branch[20]. ASTRAL quartet values and IQ-TREE concordance factors for nucleotide and amino-acid analyses are presented in the Supplementary information (Supplementary Figs. S1–S8; Supplementary Tables S5–S8).

Phylogenetic relationships within hornworts: The circumscription and relationships of classes and orders within the hornworts, Anthocerotophyta (Fig. 2 and Extended Data Figs. 1 and 4) reflect those inferred from organellar markers and a broad taxon sampling[13] except for the affinities of the monotypic Leiosporocerotales. The monophyly of subclasses and orders is typically supported by a large majority of loci, whether inferences are based on nucleotides (Extended Data Fig. 1; Supplementary Figs. S1 and S2) or amino-acid data (Extended Data Fig. 4). By contrast, the relationship of *Leiosporoceros* is ambiguous, as it is resolved

as sister to Anthocerotales (i.e., *Anthoceros*) based on nucleotide gene trees (ASTRAL) (Fig. 2 and Extended Data Fig. 1) or to all hornworts based on concatenated nucleotide data (Supplementary Fig. S5) or with ambiguous affinities based amino-acid gene trees (Extended Data Fig. 4).

The position of *Leiosporoceros* as sister to all other hornworts was previously proposed based on few organellar loci sampled for a large set of taxa[21–23] and from over 400 loci sequenced for selected hornwort placeholders[19,24]. The novel phylogenetic hypothesis in the ASTRAL analysis would impact ancestral state reconstructions for the hornwort pyrenoid: if *Leiosporoceros* is sister to all hornworts, the pyrenoid-less state would be predicted as the ancestral condition in hornworts[13], whereas under the alternative topology the presence of the pyrenoid may be ancestral in hornworts with subsequent losses in *Leiosporoceros*. Under either scenario, pyrenoids have been independently lost in all hornwort orders, and gained in the derived Dendrocerotales[13].

Phylogenetic relationships within liverworts: The earliest split within liverworts segregates the Haplomitriopsida (21 spp.) from the ancestor to the Marchantiopsida (mostly complex thalloid taxa, ca. 543 spp.) and the Jungermanniopsida (simple thalloid and leafy liverworts, over 6870 spp.), a topology supported by a small majority of loci (Fig. 2; Extended Data Figs. 2 and 5). Within the three classes, ordinal circumscriptions and relationships generally reflect prevailing interpretations[14,25–28], with most backbone nodes supported by a majority of loci and high posterior probabilities (Fig. 2 and Fig. 3; Extended Data Figs. 2 and 5).

The Haplomitriopsida comprise plants with leaf-like appendages, stems secreting copious mucilage and one primary androgonial initial in early ontogeny[29]. The earliest split in the Marchantiopsida segregates the Marchantiidae (complex thalloids) from the Blasiidae, a lineage of two simple thalloid species with endophytic cyanobacteria[30,31]. The Marchantiidae typically develop a complex thallus with air chambers, four primary androgonial initials in early ontogeny, and unlobed sporocytes[29]. The ordinal relationships within the Marchantiidae vary in support (Fig. 2 and Fig. 3; Extended Data Figs. 2 and 5). The Neohodgsoniales comprise a single species from New Zealand, diagnosed by a uniquely branched carpocephalum, and mark another deep split in the subclass[27]. The Sphaerocarpales comprise mostly taxa with leafy-like gametophytes and are sister to the Marchantiales, although not supported by most gene trees (Fig. 2 and Fig. 3; Extended Data Figs. 2 and 5). The Marchantiales contain the majority of the species of the class (ca. 497 spp.), including the model species *Marchantia polymorpha*[32].

The Jungermanniopsida include species developing simple thalloid or leafy vegetative bodies, all with antheridia developed from two primary androgonial initials in early ontogeny and with lobed sporocytes[29]. The Jungermanniopsida are typically accommodated in three subclasses, whose monophyly and relationships are not consistently resolved (Figs. 2 and 3) perhaps due to ancient introgression[31]. The Pelliidae comprise two robustly monophyletic orders (i.e., Pallaviciniales and Pelliales) and the Fossombroniales, which are supported by most nucleotide gene trees but only a small plurality of amino-acid loci (Extended Data Figs. 2 and 5). The relationships among the three orders are congruent only among a plurality of gene trees (Extended Data Figs. 2 and 5), with the paraphyly of the subclass caused by the resolution of the Pelliales sister to all other Jungermanniopsida based on

nucleotide data[23] (Figs. 2 and 3; Extended Data Fig. 2) versus sister to other Pelliidae based on amino-acid data with ambiguous signal (Extended Data Fig. 5). Such conflicting topologies were previously recovered based on nucleotide-based nuclear transcriptome and mitochondrial data[24], and plastid data[28,33], respectively, and may reflect a rapid divergence of the Pelliidae, ancient introgression, incomplete lineage sorting and subsequent saturation in nucleotide data.

The Metzgeriidae compose a robustly monophyletic group comprising the Metzgeriales and Pleuroziales (Fig. 2; Extended Data Figs. 2 and 5), as previously resolved based on a few DNA loci[25,34,35], and genomic, transcriptomic and organellar data[28,33]. The monophyly of the Metzgeriidae is supported by the unique shared lenticular apical cell giving rise to the bilaterally symmetric and thalloid body of the Metzgeriales and the leafy stem of the Pleuroziales[23].

The vast majority of liverworts (ca. 6160 spp.) belong to the well supported clade Jungermanniidae or true leafy liverworts (Figs. 2 and 3; Extended Data Figs. 2 and 5). A shared ancestry of the Ptilidiales and Porellales *sensu lato*, as inferred from nuclear nucleotide data (Fig. 2; Extended Data Fig. 2) was recently argued for based on phylotranscriptomic and plastid evidence[33]. By contrast, our amino-acid data resolve the Ptilidiales as sister to the Jungermanniales *s. lato* (Extended Data Fig. 5), a hypothesis also supported by mitochondrial data[23,33] and prior plastid-based inferences[25,28]. A majority of genes recover the monophyly of the Porellales *s. lato*, which we propose to accommodate into three resurrected and two new orders (Table 1), each of pre-Cretaceous origin: Frullaniales, Jubulales, Lejeuneales Porellales, and Radulales (Fig. 2; Extended Data Figs. 2 and 5). The Frullaniales (ca. 599 spp.) and Lejeuneales (ca. 1900 spp.) comprise two of the most species-

rich families of liverworts characteristic of epiphytic communities, particularly in tropical rainforests[15].

Within the Jungermanniales *s. lato*, the deepest splits giving rise to the main lineages are estimated to have occurred in or prior to the Triassic, and we therefore propose to recognize these at the ordinal level, resurrecting Perssoniellales[36], Lepidoziales and Lophoziales and erecting Myliales (Table 1). The Perssoniellales (ca. 88 spp.) emerged from the earliest split (Fig. 2) in the Carboniferous (Fig. 3) and are sister to the common ancestor shared by the remaining others. The Myliales (5 spp.) mark the next split based on nucleotide data (Figs. 2 and 3; Extended Data Fig. 2) or are sister to the Lophoziales only, based on amino-acid data, although with low support (Extended Data Fig. 5). Either resolution is incongruent with *Mylia* sister to the Jungermanniales *s. str*. based on nuclear transcriptomic and organellar data[33], a hypothesis based, however, on a mislabeled specimen (Y. Liu, pers. com. March 2023).

A majority of nucleotide, and at least a plurality of amino-acid, gene trees resolve the remaining orders of the Jungermanniales *s. lato*, i.e., the Lophoziales (ca. 611 spp.), Lepidoziales (ca. 1943 spp.) and Jungermanniales *s. str*. (ca. 565 spp.) as monophyletic (Extended Data Figs. 2 and 5, respectively). All three suborders are highly heterogenous in terms of leaf morphology (2–4 lobes), branching patterns, form, and position of gametangia[37]. The sister-group relationship of the latter two suborders most recently supported by nuclear transcriptomic and organellar data[33], emerges here also from a near majority of nucleotide loci but only a weak plurality of amino-acid loci (Extended Data Figs. 2 and 5, respectively). The resolution within suborders seems to vary, especially within species-rich families

(e.g., Lepidoziaceae) and may point to a period of rapid diversification (Extended Data Figs. 2 and 5).

Phylogenetic relationships within mosses: The phylogenetic structure in mosses (Fig. 2; Extended Data Figs. 3 and 6) is congruent with most current supraordinal circumscriptions and ordinal relationships and shaped primarily by innovations in sporangial dehiscence, peristome architecture and development, and by vegetative body plant organization relative to sex organ position[29,38]. The circumscription and relationships of classes and subclasses sensu[29,38,39] are typically supported by a majority or a plurality of loci (Fig. 2; Extended Data Fig. 3) or their amino-acid translations (Extended Data Fig. 6), while concordance among nucleotide loci is typically low for clades following the initial splits within the Bryophyta (Fig. 2; Supplementary Tables S5 and S7).

The current classification[11] accommodates mosses into four subdivisions, which are here recovered as emerging from the deepest splits, with the Takakiophytina sister to all other extant mosses, followed by the Sphagnophytina and the Andreaeophytina, which comprise the two lineages of lantern mosses (i.e., Andreaeales and Andreaeobryales) and are sister to the remaining mosses composing the Bryophytina (Fig. 2; Extended Data Figs. 3 and 6). The latter comprise species potentially developing stomata on their sporangia and a peristome, a set of teeth lining the sporangial mouth and controlling spore dispersal[12]. Thus, the lack of stomata in the other subdivisions is considered to result from independent losses[5], which given the topology occurred independent in all three bryophyte lineages.

Mosses developing peristome teeth made of whole cells (i.e., nematodontous peristome, Fig. 1K) compose a monophyletic group, the Polytrichopsida *s. str.*, as previously suggested[38]. The monospecific Oedipodiales were resolved either as sister to all peristomate mosses in a small plurality of nucleotide gene trees (Fig. 2, Extended Data Fig. 3) and congruent with signal from organellar loci[38], or only to the Polytrichopsida in a small plurality of amino-acid gene trees[40] (Extended Data Fig. 6). The ambiguous placement of the Oedipodiales from nucleotide data likely emerges from a combination of a relatively rapid divergence (Fig. 3) and saturation in nucleotide substitution, as the more conserved amino-acid data more robustly resolve the Oedipodiales as sister to the Polytrichales and Tetraphidales, similarly to inferences from a distinct set of hundred nuclear loci[38].

The remaining mosses (i.e., Bryopsida) typically develop a peristome composed solely of cell plates rather than whole cells (Fig. 1L). Such joined and hence articulate teeth lining the sporangial or capsule mouth upon dehiscence likely constitute a key innovation that optimizes and controls spore release and is developed by the vast majority of mosses. Several arthrodontous peristome types arise from distinct developmental sequences[12] and these largely define monophyletic groups[38]. However, the resolution of *Catoscopium* as sister to most Dicranidae may call for an amendment of *Dicranum*-peristome type diagnosis[41]. Although mature peristomes may be variably reduced, especially along environmental gradients[42], the fundamental architecture and ontogeny seem highly conserved during the diversification of mosses.

The vast majority of mosses belong to the Bryidae, a lineage diagnosed by its double peristome of alternating inner and outer teeth[43]. The subclass comprises the

most speciose superorder of mosses, the Hypnanae or pleurocarpous mosses (ca. 4903 spp.), which are characterized by a homogenous anatomy of their midrib, the lateral development of female sex organs, and hence of the sporophyte on the maternal gametophyte[44,45]. The Hypnanae comprise five orders (i.e., Hypnodendrales, Ptychomniales, Hypopterygiales, Hookeriales and Hypnales), whose relationships match those previously recovered[38] but are here, too only supported by a plurality of loci (Fig. 2; Extended Data Figs. 3 and 6). While a lateral shift of the sex organs and the associated shift to monopodial growth has occurred in other moss lineages[46], such as the Orthotrichales, the persistence of lateral female sex organs in all Hypnanae suggest that this trait is either under strong genetic constraint or selection (see [47,48]). Within the Hypnales, the most diverse order of mosses[49] the backbone relationships are typically shared only by a plurality of gene trees (Fig. 2; Extended Data Figs. 3 and 6), likely reflecting a rapid early radiation of the order[50]. The recurrent phylogenetic pattern of species-rich families being either paraphyletic due to the inclusion of additional, morphologically distinct lineages, or polyphyletic following their phylogenetic fragmentation, and the resolution of various species poorer lineages across the backbone phylogeny, reveals that morphological traits, and primarily the vegetative ones, are evolutionarily highly labile within the Hypnales. Transformations of putative homologous traits appear highly homoplasious, and potentially correlated, yielding morphologically highly heterogenous clades. Such homoplasy may even span across subclasses, as reflected by *Sorapilla*, the sole member of Sorapillaceae, and which was originally placed in Dicranidae, but was then moved to the Hypnales[51]. Based on the first DNA sequences obtained for this genus, we resolve the family in the Dicranidae as proposed earlier[52,53] but in an isolated position within the Dicranalean grade (Fig. 2;

Extended Data Figs. 3 and 6), prompting the proposal for a new order, Sorapillales (Table 1).

The Hypnanae emerged from the acrocarpous Bryidae that typically develop terminal sex organs. The Bryidae are consistently recovered as paraphyletic across all present (Fig. 2; Extended Data Figs. 3 and 6) and prior[38] analyses. While all orders are recovered with strong support, the relationships among them are typically supported only by a plurality of loci (Fig. 2; Extended Data Figs. 3 and 6). The relationships among the Rhizogoniales, Orthotrichales, Orthodontiales and Aulacomniales inferred here from nucleotide data (Fig. 2; Extended Data Fig. 3) match those previously proposed[38] based on amino-acid sequences. However, the present protein-based topology (Extended Data Fig. 6) differs in that a clade comprising some members of the Rhizogoniales, along with *Hymenodontopsis*, a member of the Aulacomniaceae, are sister to the Hypnanae, whereas the Orthotrichales, Orthodontiales and Aulacomniales, and *Goniobryum* (a member of the Rhizogoniaceae) compose a single lineage sister to the Rhizogoniales and Hypnanae (Extended Data Fig. 6). The relationships of these orders are in all cases supported only by a small plurality of loci. Furthermore, inferences from nucleotide versus amino-acid data resolve incongruent circumscriptions of the Rhizogoniales. *Calomnion*, a genus of a few South Pacific Island species[54] is reconstructed as sister to the Hypnanae except Hypnodendrales or all Hypnanae based on nucleotide versus amino-acid data, respectively (Fig. 2; Extended Data Figs. 3 and 6). In none of the alternative topologies are the relationships supported by a majority of loci, and hence the circumscription of the Rhizogoniales remains uncertain. The early diversification of the Bryidae gave rise to the Bartramiales, Bryales, Hedwigiales, and Splachnales, which compose robust lineages but of uncertain relationship. The

Helicophyllaceae (Hedwigiales), diagnosed by plagiotropic shoots and dimorphic leaves[55], are robustly resolved as sister to the Bartramiaceae (Figs. 2 and 3; Extended Data Figs. 3 and 6; see also [56]).

Within the Dicranidae, the sister group to the Bryidae, the relationships are congruent with previous hypotheses[33] and strengthen the hypothesis of a broadly polyphyletic Dicranales. The earliest splits within the subclass gave rise to the Catoscopiales, followed by the here erected Distichiales and Flexitrichales (Table 1). The later holds only the Flexitrichaceae, a family here formally recognized (Table 1), and is likely sister to a here not sampled Scouleriales (sensu [57]; Fig. 2). The next split yields the Grimmiales, sister to the clade composed of the Archidiales, the dicranalean grade and the Pottiales (Fig. 2; Extended Data Figs. 3 and 6). The circumscription of the Archidiales Limpr. is here broadened to include the Micromitriaceae and Leucobryaceae, as the Archidiaceae are nested between the latter two families (Fig. 2; Extended Data Figs. 3 and 6)[58].

The Dicranales are consistently resolved as a grade leading to the well supported Pottiales (Fig. 2; Extended Data Figs. 3 and 6), a hypothesis congruent with prior phylogenetic studies[38,58,59]. To integrate the phylogenetic resolution of the dicranalean grade into the current classification, we propose to restrict the Dicranales (Fig. 2) to only the Dicranaceae, Calymperaceae, Fissidentaceae and Octoblepharaceae, and accommodate the remaining families, which all have an origin no later than the Jurassic (Fig. 3), in the Amphidiales, Bruchiales, Ditrichales, Erpodiales, Eustichiales, Pleurophascales and Rhabdoweisiales (Table 1). Despite these systematic novelties, various families of the Dicranales *s. lato* remain unassigned (e.g., Amphidiaceae, Distichiaceae, etc.) awaiting further study.

Our phylogenomic inferences confirm that the Timmiidae, restricted to *Timmia* characterized by a unique peristomial architecture[60], compose the sister lineage to the ancestor of the Dicranidae and Bryidae[38]. The Funariidae, which include the model taxon *Physcomitrium patens*[61] along with the Diphysciidae and Buxbaumiidae, each with a distinct peristome type compose the basal grade within the Bryopsida. Thus, the main transformations of the arthrodontous peristome, yielding the various fundamental types, occurred during the Permian or even late Carboniferous (Fig. 3) rather than in the first half of the Paleozoic as previously proposed (Laenen et al. 2014).

500 million years of bryophyte diversification

Divergence time estimates of the first comprehensive phylogenomic reconstructions of bryophytes confirm that they arose in the Ordovician[16]. Speciose lineages arose during the diversification of angiosperms in the Cretaceous (Fig. 3; Extended Data Figs. 7, 10). The common ancestor to extant lineages of mosses and liverworts is traced to 420 [416–424] Ma and 447 [444–450] Ma, respectively, which is consistent with recent estimates[8,13,15,16,44]. The lineage through time plots (Fig. 3B) suggest a rather steady diversification of both lineages over the last 400 My with a higher net moss diversification near mid Cretaceous. The average crown age of orders as recognized here across all three bryophyte lineages is 150.5 Ma (SD 70 Ma) (Fig. 3C; Supplementary Table S10). The crown age of the most species rich bryophyte order, the Hypnales (491 genera, ca. 4150 species) is 129 [78–173] Ma, and thus younger than previously estimated[62]. The origin of mosses and liverworts (419–447 Ma, crown group Setaphyta) seem to be slightly older than that of extant lycophytes and their sister group, the euphyllophytes[16]. The age of most bryophyte

orders coincides with the diversification of angiosperms during the Late Jurassic and Cretaceous[63].

Our estimates of family stem ages suggest that most bryophyte families (63% of families, n=166) originated during the Cretaceous (65 families) and Jurassic (40 families). Extant bryophyte families (crown ages, n=80) diversified predominantly during the Late Cretaceous (66–102 Ma, 27 families) and the early Cretaceous (103–145 Ma, 18 families) and the Cenozoic (–65 Ma, 26 families). The average crown age of bryophyte families is 98 Ma (SD 51 Ma) (Extended Data Fig. 10; Supplementary Table S10; Supplementary Fig. S9). In mosses, the crown age of the Pottiaceae (77 genera, ca. 1,209 species) is estimated at 133.3 [115–150] Ma and the Orthotrichaceae (24 genera, ca. 900 species) started to diversify around 139.6 [106–169] Ma. Within liverworts, the diversification of the hyperdiverse Lejeuneaceae (ca. 88 genera, ca. 1900 species) began around 149 [116–188] Ma while that of the Lepidoziaceae (31 genera, ca. 703 species) dates to 121 [114–166] Ma. As previously suggested for bryophyte genera[14], bryophyte diversity may have accrued during the Cretaceous and Cenozoic[14] (Fig. 3C). Our analyses support the Cretaceous terrestrial revolution[63,64] wherein the majority of bryophyte families diversified during this period (Fig. 3; Extended Data Fig. 10; Supplementary Table S10; Supplementary Fig. S9) contributing to an explosive radiation of life. The Cretaceous expansion of the angiosperm canopy and diversification of leptosporangiate ferns[65] potentially provided novel habitats for bryophytes to diversify in tropical and subtropical areas. In addition, global and local extinctions, and the climatic fluctuations during the Cretaceous and Cenozoic may explain the burst of diversity in lineages occupying new niches in arid regions (e.g., Pottiales,

Marchantiales) or open areas (e.g., Funariales, Polytrichales) before the explosive diversification of angiosperms and ferns.

Conclusions

Bryophytes are the second-most diverse group of land plants, compose the sister group to extant vascular plants[8,24] and contribute significant ecosystem functions in communities where they are abundant. Bryophytes are thus critical to understand the polarity of character transformations early in the evolution of land plants, and contemporary ecological processes, in particular, local and global nutrient flows. In parallel to the loss of complexity of the vascular plant gametophyte, this puts renewed importance on comparative studies of gametophyte morphology and function. The ordinal-level phylogeny of the bryophytes, based on the GoFlag408 probe set, provides an expandable resource upon which to build such studies.

Our results are largely consistent with previous efforts based on fewer loci or representative taxon sampling, with some interesting exceptions (Fig. 2) suggesting that the bryophyte phylogenetic studies are converging on a relatively stable set of relationships. The incongruence found in several nodes along the backbone implies that different genes coalesce to variable and conflicting topologies, especially in recent radiations (e.g., Hypnales), or are remnants of potential ancient introgressions[33] (Fig. 3; Extended Data Figs. 8 and 9) or incomplete lineage sorting. The current challenge facing the community is to fill in unsampled genera, species, or populations of focal taxa. At shallower phylogenetic depth, the data could be expanded to the flaking intron and spacer regions that are generally more variable

than the exonic regions, and hence suitable for resolving population genomic problems within or between populations of single species, or groups of closely related species. The growing GoFlag 408 database of sequences used here, and in other studies, provides a sturdy scaffold in which to place more focused studies.

Methods

Taxon sampling

We sampled in total 531 bryophyte species belonging to 499 genera (Supplementary Table S3), comprising 362 moss species representing 338 genera (34 %); 159 liverwort species that can be assigned to 151 genera (37 %), and 12 hornwort species from 10 genera (100 %).Sampling percentage values were calculated using recent checklists and classification literature[66–68]. Hornworts were assumed to be the sister group of the other two bryophyte clades based on [24].

DNA Extraction

We used the modified cetyltrimethylammonium bromide (CTAB) extraction protocol[69] described in [19] for most of the samples. This includes lysing the cells by centrifuging them and performing two rounds of chloroform/isoamyl 24:1 wash followed by cold isopropanol precipitation and an ethanol 70% wash. Finally, we added 2 µl of 10 mg/Ml ml RNase A (QIAGEN, Valencia, California, United States) to remove RNA contamination between chloroform washes. For a few specimens (Lejeuneaceae)

the Invisorb Spin Plant Mini Kit (Stratec Molecular GmbH, Berlin, Germany) was used following the kit protocol.

Target Enrichment and Sequencing Assembly

We generated a multi-locus nuclear sequence dataset with a target enrichment approach using the GoFlag probe sets. We assembled published data from 36 samples generated using the GoFlag 451 probe set and generated new data from 497 samples using the GoFlag 408 probe set, an optimized subset of the GoFlag 451 probe set consisting of 53,306 probes covering 408 exons from single or low copy nuclear loci. The library preparation, target enrichment, and sequencing were done by RAPiD Genomics (Gainesville, FL USA) using protocols described in [19], with the enriched, pooled libraries sequenced on an Illumina HiSeq 3,000 platform (Illumina; 2 × 100 bp).The paired end raw reads are available in the NCBI SRA database. We assembled phylogenetic sequence alignments for each locus using the iterative baited assembly pipeline[19]. In some loci, the pipeline retains more than copy per sample, where the Bridger[70] assembler interprets greater than simple allelic variation. To control this, we removed all copies of a sample in a locus alignment (script "rmall.pl"). Second, we removed any columns in the alignments that had nucleotide data from fewer than ten samples in all output PHYLIP files. We also pruned out sequences associated with excessively long branches in the locus trees. First, we inferred maximum likelihood (ML) trees from the locus alignments using RAxML using the GTR CAT model, and we rooted the resulting gene trees with Newick Utilities[71] using the hornworts as the outgroup. We eliminated one locus for which hornworts were not monophyletic. For the others, we calculated the root to tip

distance for each taxon and pruned out any sequences that had a root to distance >3 standard deviations more than the average for that locus. This removed 750 out of 178,650 sequences. We then for each locus examined the trees with branch lengths >1 and removed 35 additional long branch sequences. All loci correspond to exons, and some which are part of the same gene[19]. Thus, to create gene alignments, we concatenated any loci found in the same gene, resulting in 228 gene alignments that were used in our analyses. We also created amino-acid alignments for each gene. To do this, we took the original locus alignments and removed any columns sequence alignments with only one nucleotide, most likely representing sequencing error. We used AliView[72] to make edits by hand to put the alignments in frame; usually this required minimal editing to getting the alignments in line. We then saved the corresponding amino-acid alignments and concatenated the loci from the same gene.

Phylogenomic analyses

We performed Maximum Likelihood phylogenetic inferences of the concatenated nucleotide dataset implemented in IQ-TREE v.2.1[73]. Loci located within the same gene were concatenated and the dataset was partitioned by genes (228 genes) and were used for nucleotide and amino-acid analyses. The best-scoring ML tree and a rapid bootstrap analysis with 100 replicates was run. In all cases a GTRGAMMA model of sequence evolution was chosen. Moreover, we used IQ-TREE v.2.1[73] for phylogenetic inference on the translated matrix dataset (into amino-acids), with “-S option” that load all alignment files within the directory. We performed auto model

selection (ModelFinder) and tree inference separately for each gene. Branch support was assessed using ultrafast bootstrapping (1000 replicates)[74].

We conducted species tree analyses using ASTRAL-III v.5.7.7[75]. Gene trees were estimated in RAxMLv.8.2.9[76,77] under the following settings for the nucleotide dataset: the default RAxML tree search algorithm (-f d) was implemented and a GTRGAMMA model selected. The loci belonging to the same gene were combined prior to the gene tree estimation, resulting in 228 unrooted gene trees. For amino-acids dataset gene trees were estimated in IQ-TREE v.2.1, with "-S option" (see above). ASTRAL-III was employed for species tree inference on both gene tree datasets using the default settings and computing local posterior probabilities[78] as well as quartet scores for all three resolutions per branch (-t 8). The resulting ASTRAL topologies were annotated with quartet support values[78] for the main topology (q1), the first alternative topology (q2), and the second alternative topology (q3). We also used the built-in functionality of ASTRAL to compute the percentage of gene trees that agreed with each branch in the species tree, by finding the average number of gene-tree quartets defined around the branch (choosing one taxon from each side) that were congruent with the species tree. Similar phylogenetic analyses were conducted on the translated matrix (into amino-acids). We used DiscoVista[79] to visualize the results.

In addition to bootstrap (IQ-TREE) and local posterior probabilities (ASTRAL), we implemented the gene (gCF) and site (sCF) concordance factors to investigate topological conflict around each branch of the species tree for the nucleotide and amino-acid datasets in IQ-TREE, using the "–gcf and –scf " options[20], particularly for

the backbone nodes. Likewise, we compared the species and gene trees generated with ASTRAL (gCGAst, sCFAst, sDFPAst) and IQ-TREE (maximum likelihood, gCGmL, sCFmL, gDFPmL) to evaluate possible divergences. These analyses measured every branch of the species tree; the gCF and sCF represents the percentage of decisive gene trees and sites. The program also estimates gDFP (gene discordant factor due to paraphyly) or the gene discordance factor due to lack of information in the genes or paraphyly of the quartet. For measures of support gene concordance factor/site concordance factor (gCF/sCF) was categorized as follows" weak < 33, moderate 33–50, strong > 50 (following [20,80]). Using the ASTRAL output, we analyzed whether the discordance among gene trees or sites regarding the neutral ILS model implemented in IQ-TREE. We carried out χ^2 tests comparing the number of trees or sites supporting discordant topologies with roughly equal quartet values. Under the assumption of ILS, the discordant topologies should be supported by an equal number of gene trees or sites (Supplementary Table 12). Equal quartets, gcf or scf (~33%) for the tree quartets point out to incomplete lineage sorting or ancient introgression[20]. We performed correlation analyses between branch lengths, divergence times (see below) and concordance factor values using linear regressions.

Divergence time estimation

Divergence time estimation was performed in treePL[81] according to the analysis guidelines of [82]. The best-ML tree as input for treePL was selected from the maximum likelihood analysis (see above). In order to be able to infer node bars on the dated tree, a set of bootstrap replicates were run through the

"Bootstrap+Consensus" workflow of RAxML-HPC2 on XSEDE on the CIPRES Science Gateway[83], whereby the best ML tree served as constraint, the option to print branch lengths on the BS replicates was selected, a partition scheme by genes (i.e., loci were grouped together according to their relatedness to genes) was implemented as well as a GTR+G substitution model and 1000 bootstrap iterations. All trees were rooted with hornworts set to be the sister group of other bryophytes, using the program pxrr in phyx[84] that was also used in the dating analysis. We calibrated 16 liverwort and 13 moss nodes stemming from fossil evidence (Supplementary Table S2) and implemented a maximum age constraint of the root of 515 Ma[16]. Priming and cross-validation analyses were performed using the best-ML tree and all 29 calibrations. Best optimization parameters were indicated as the follows: opt = 2, optad = 2, optcvad = 5. Cross-validation used these parameters and was done four times, indicating stable values of a smoothing parameter = 10. To obtain confidence intervals on the dated tree, we ran the treePL analysis with the bootstrap replicates using the same calibration, optimization and cross-validation values as outlined above. The set of trees was summarized in TreeAnnotator v.2.6.6[85]; (part of the BEAST package) with mean node heights and 0% of burnin. Trees were visualized in FigTree v.1.4.3[86]. Lineage-through-time plots were conducted on the treePL chronogram for all bryophyte taxa together, as well as liverworts and mosses separated using the R-package "ape"[87,88]. We visualized the temporal distribution of order and family ages using the average stem and crown age. Monotypic families or orders were excluded from the calculations (Supplementary Table S10). Bryophyte species number were obtained from [66–68].

Absolute rates were estimated with the same calibrations and targeted ML trees using r8s[89]. Among-lineage rate variation, as expected across such a dataset,

is high. The lowest absolute substitution rate in mosses characterizes the Orthodontiales (1.34×10^{-04} subst/site/Ma) and the highest the Polytrichales (5.44×10^{-04} subst/site/Ma). In liverworts, the variation spans from 3.53×10^{-04} subst/site/Ma in the simple thalloid Pallaviciniales to 7.85×10^{-04} subst/site/Ma in the complex thalloids (Marchantiopsida,) (Fig. 3; Supplementary Table S9). The rate variation observed in our dataset set the stage to test specific hypotheses correlating natural history traits (e.g., perennial vs annual taxa) and molecular rates across genes and all bryophyte groups.

Data Availability Section

All bryophyte gene sequences, alignments for each gene and concatenated alignments will be available from FigShare.

Acknowledgements

We thank all the herbaria that provided specimens. Funding was provided by the NSF collaborative project “Building a Comprehensive Evolutionary History of Flagellate Plants” (DEB #1541506 to JG Burleigh, EC Davis, S McDaniel, and EB Sessa, and #1541545 to M von Konrat). A.A. acknowledges the financial support by the University of Padova (BIRD 173749/17). BG acknowledges DEB-1753811. JCVA acknowledges the Canada Research Chair (950-232698); the CRNSG- RGPIN 05967–2016 and the Canadian Foundation for Innovation (projects 36781, 39135)

Author contributions

G.B., S.M., D.B., G.P.-B., J.B., B.G., J.C.V.A. conceptualized the study.

B.G, J.C.V.A. wrote the first draft.

G.B., S.G., K.S.R., D.Q., J.L., F.L., I.D., E.S., J.B., D.B., G.P.-B., B.G., J.C.V.A. participated in the final reviewing and editing.

A.B, A.M.S.P., A.S.-V., C.Z., C.D., D.C.C., I.D., J.J.L., J.L., L.L., M.v.K., S.C., S.H., D.L., L.E., L.L.F., P.L., R.G., G.E.L., K.F., J.B., G.P.-B., S.M., D.B., J.B., J.C.V.A. participated in the specimen collections.

L.L., L.E., G.E.L., J.B., J.C.V.A. participated in data collection and laboratory work. **G.B., J.B., G.P.-B., A.M.S.P., B.G., J.C.V.A.** performed the analyses.

G.B., C.D., E.S., S.M., J.C.V.A. procured funding.

Additional Information

References

1. Puttick, M. *et al.* The interrelationships of land plants and the nature of the ancestral embryophyte. *Curr. Biol.* **28**, 733-745.e2 (2018).

2. Sousa, F., Foster, P., Donoghue, P., Schneider, H. & Cox, C. Nuclear protein phylogenies support the monophyly of the three bryophyte groups (Bryophyta Schimp.). *New Phytol.* **222**, 565–575 (2019).

3. Rich, M. & Delaux, P.-M. Plant evolution: when Arabidopsis is more ancestral than Marchantia. *Curr. Biol.* **30**, R642–R644 (2020).

4. Cammarata, J., Morales Farfan, C., Scanlon, M. & Roeder, A. Cytokinin–CLAVATA cross-talk is an ancient mechanism regulating shoot meristem homeostasis in land plants. *Proc. Natl. Acad. Sci.* **119**, 1–11 (2022).

5. Harris, B. J., Harrison, C. J., Hetherington, A. M. & Williams, T. A. Phylogenomic Evidence for the Monophyly of Bryophytes and the Reductive Evolution of Stomata. *Curr. Biol.* **30**, 1–12 (2020).

6. Bennett, T. *et al.* Plasma membrane-targeted pin proteins drive shoot development in a moss. *Curr. Biol.* **24**, 2776–2785 (2014).

7. Lavy, M. *et al.* Constitutive auxin response in Physcomitrella reveals complex interactions between Aux/IAA and ARF proteins. *Elife* **5**, 1–22 (2016).

8. Harris, B. J. *et al.* Divergent evolutionary trajectories of bryophytes and tracheophytes from a complex common ancestor of land plants. *Nat. Ecol. Evol.* (2022) doi:10.1038/s41559-022-01885-x.

9. Porada, P., Weber, B., Elbert, W., Pöschl, U. & Kleidon, A. Estimating impacts of lichens and bryophytes on global biogeochemical cycles. *Global Biogeochem. Cycles* **28**, 71–85 (2014).

10. Stuart, J. *et al.* Host identity as a driver of moss-associated N2 fixation rates in Alaska. *Ecosystems* **24**, 530–547 (2021).

11. Porada, P., Weber, B., Elbert, W., Pöschl, U. & Kleidon, A. Estimating global

carbon uptake by lichens and bryophytes with a process-based model. *Biogeosciences* **10**, 6989–7033 (2013).

12. Goffinet, B., Buck, W. & Shaw, J. Morphology, anatomy, and classification of the Bryophyta. in *Bryophyte biology* 55–138 (Cambridge University Press, 2009).

13. Villarreal, J. C. & Renner, S. Hornwort pyrenoids, carbon-concentrating structures, evolved and were lost at least five times during the last 100 million years. *Proc. Natl. Acad. Sci.* **109**, 18873–18878 (2012).

14. Laenen, B. *et al.* Extant diversity of bryophytes emerged from successive post-Mesozoic diversification bursts. *Nat. Commun.* **5**, 5134 (2014).

15. Feldberg, K. *et al.* Epiphytic leafy liverworts diversified in angiosperm-dominated forests. *Sci. Rep.* **4**, 5974 (2014).

16. Morris, J. L. *et al.* The timescale of early land plant evolution. *Proc. Natl. Acad. Sci.* **115**, E2274–E2283 (2018).

17. Feldberg, K. *et al.* Checklist of fossil liverworts suitable for calibrating phylogenetic reconstructions. *Bryophyt. Divers. Evol.* **43**, 14–71 (2021).

18. Ignatov, M. S. & Maslova, E. V. Fossil mosses: What do they tell us about moss evolution? *Bryophyt. Divers. Evol.* **43**, 72–97 (2021).

19. Breinholt, J. W. *et al.* A target enrichment probe set for resolving the flagellate land plant tree of life. *Appl. Plant Sci.* **9**, 1–28 (2021).

20. Minh, B. Q., Hahn, M. W. & Lanfear, R. New Methods to Calculate

Concordance Factors for Phylogenomic Datasets. *Mol. Biol. Evol.* **37**, 2727–2733 (2020).

21. Duff, J., Villarreal, J. C., Cargill, C. & Renzaglia, K. Progress and challenges toward developing a phylogeny and classification of the hornworts. *Bryologist* **110**, 214–243 (2007).

22. Villarreal, J. C., Cusimano, N. & Renner, S. Biogeography and diversification rates in hornworts: The limitations of diversification modeling. *Taxon* **64**, 229–238 (2015).

23. Bell, D. *et al.* Organellomic data sets confirm a cryptic consensus on (unrooted) land-plant relationships and provide new insights into bryophyte molecular evolution. *Am. J. Bot.* **107**, 91–115 (2020).

24. Leebens-Mack, J. *et al.* One thousand plant transcriptomes and the phylogenomics of green plants. *Nature* **574**, 679–685 (2019).

25. Forrest, L. L. *et al.* Unraveling the evolutionary history of the liverworts (Marchantiophyta): Multiple taxa, genomes and analyses. *Bryologist* **109**, 303–334 (2006).

26. Dong, S. *et al.* Plastid genomes and phylogenomics of liverworts (Marchantiophyta): Conserved genome structure but highest relative plastid substitution rate in land plants. *Mol. Phylogenet. Evol.* **161**, 107171 (2021).

27. Villarreal, J. C., Crandall-Stotler, B., Hart, M., Long, D. & Forrest, L. Divergence times and the evolution of morphological complexity in an early land plant lineage (Marchantiopsida) with a slow molecular rate. *New Phytol.*

209, 1734–1746 (2016).

28. Yu, Y. *et al.* Chloroplast phylogenomics of liverworts: a reappraisal of the backbone phylogeny of liverworts with emphasis on Ptilidiales. *Cladistics* **36**, 184–193 (2020).

29. Crandall-Stotler, B. J., Stotler, R. E. & Long, D. G. Morphology and classification of the Marchantiophyta. in *Bryophyte Biology* (eds. Shaw, B. & Goffinet, A. J.) 1–54 (Cambridge University Press, 2009).

30. Liaimer, A., Jensen, J. & Dittmann, E. A genetic and chemical perspective on symbiotic recruitment of cyanobacteria of the genus Nostoc into the host plant Blasia pusilla L. *Front. Microbiol.* **7**, 1–16 (2016).

31. Renzaglia, K. S. & Duckett, J. G. Spermatogenesis in Blasia pusilla: from young antheridium through mature spermatozoid. *Bryologist* **90**, 419 (1987).

32. Bowman, J. L. *et al.* Insights into Land Plant evolution garnered from the Marchantia polymorpha Genome. *Cell* **171**, 287-304.e15 (2017).

33. Dong, S., Yu, J., Zhang, L., Goffinet, B. & Liu, Y. Phylotranscriptomics of liverworts: revisiting the backbone phylogeny and ancestral gene duplications. *Ann. Bot.* 1–13 (2022) doi:10.1093/aob/mcac113.

34. Davis, E. C. A molecular phylogeny of leafy liverworts (Jungermanniidae: Marchantiophyta). in *Molecular systematics of bryophytes: progress, problems and perspectives vol. 98* (eds. Goffinet, B., Hollowell, V. C. & Magill, R. E.) 61–86 (Missouri Botanical Garden, 2004).

35. He-Nygrén, X., Ahonen, I., Juslén, A., Glenny, D. & Piippo, S. Phylogeny of liverworts-beyond a leaf and a thallus. in *Molecular systematics of bryophytes: progress, problems and perspectives vol. 98* (eds. Goffinet, B., Hollowell, V. C. & Magill, R. E.) 87–118 (Missouri Botanical Garden, 2004).

36. Schljakov, R. N. On the higher taxa of liverworts—class Hepaticae s. str. *Bot. Zhurnal* **57**, 496–508. (1972).

37. Crandall-Stotler, B., Stotler, R. E. & Long, D. G. Phylogeny and classification of the Marchantiophyta. *Edinburgh J. Bot.* **66**, 155–198 (2009).

38. Liu, Y. *et al.* Resolution of the ordinal phylogeny of mosses using targeted exons from organellar and nuclear genomes. *Nat. Commun.* **10**, 1–11 (2019).

39. Goffinet, B., Buck, W. & Shaw, J. Addenda to the classification of mosses. I. Andreaeophytina stat. nov. and Andreaeobryophytina stat. nov. *Bryologist* **112**, 856–857 (2009).

40. Chang, Y. & Graham, S. W. Patterns of clade support across the major lineages of moss phylogeny. *Cladistics* **30**, 590–606 (2014).

41. Ignatov, M. S., Spirina, U. N., Ignatova, E. A., Krug, M. & Quandt, D. On the systematic position of the moss genus Catoscopium, with a new approach to the peristome reduction study. *Arctoa* **24**, 389–415 (2015).

42. Vitt, D. Adaptive modes of the moss sporophyte. *Bryologist* **84**, 166–186 (1981).

43. Goffinet, B. & Shaw, A. J. *Bryophyte biology*. (Cambridge University Press,

2009).

44. Bell, N. E., Quandt, D., O'Brien, T. J. & Newton, A. E. Taxonomy and phylogeny in the earliest diverging pleurocarps: Square holes and bifurcating pegs. *Bryologist* **110**, 533–560 (2007).

45. Huttunen, S., Bell, N. & Hedenäs, L. The Evolutionary Diversity of Mosses – Taxonomic Heterogeneity and its Ecological Drivers. *CRC. Crit. Rev. Plant Sci.* **37**, 128–174 (2018).

46. Farge-England, C. La. Growth Form, Branching Pattern, and Perichaetial Position in Mosses: Cladocarpy and Pleurocarpy Redefined. *Bryologist* **99**, 170 (1996).

47. Coudert, Y., Bell, N., Edelin, C. & Harrison, C. Multiple innovations underpinned branching form diversification in mosses. *New Phytol.* **215**, 840–850 (2017).

48. Coudert, Y. *et al.* Three ancient hormonal cues co-ordinate shoot branching in a moss. *Elife* **4**, 1–26 (2015).

49. Crosby, M. R., Magill, R. E., Allen, B. & He, S. A checklist ofthe mosses. *Missouri Bot. Gard.* (1999).

50. Shaw, A., Cox, C., Goffinet, B., Buck, W. & Boles, S. Phylogenetic evidence of a rapid radiation of pleurocarpous mosses (Bryophyta). *Evolution (N. Y).* **57**, 2226–2241 (2003).

51. Meagher, D., Cairns, A., Seppelt, R. & Grixti, M. A re-evaluation of the

morphology of Sorapilla (Bryophyta: Sorapillaceae) based on Sorapilla papuana. *Aust. Syst. Bot.* **33**, 427–435 (2020).

52. Lin, S. H. A taxonomic revision of Phyllogoniaceae (Bryopsida). part I J. Taiwan Mus. 臺灣省立博物館半年刊 **37**, 1–54 (1983).

53. Vitt, D. H. Classification of the Bryopsida. *New Man. Bryol.* 696–759 (1984).

54. Vitt, D. H. The genus Calomnion (Bryopsida): taxonomy, phylogeny, and biogeography. *Bryologist* **98**, 338 (1995).

55. Vitt, D. H. The New Zealand species of the pantropical genus Macromitrium (Orthotrichaceae Musci) taxonomy, phylogeny and phytogeography. *J. Hattori Bot. Lab.* 1–94 (1983) doi:10.18968/jhbl.54.0_1.

56. Buchbender, V. *et al.* Phylogenetic reconstructions of the Hedwigiaceae reveal cryptic speciation and hybridisation in Hedwigia. *Bryophyt. Divers. Evol.* **36**, 1 (2014).

57. Fedosov, V. E., Fedorova, A. V., Fedosov, A. E. & Ignatov, M. S. Phylogenetic inference and peristome evolution in haplolepideous mosses, focusing on Pseudoditrichaceae and Ditrichaceae s. l . *Bot. J. Linn. Soc.* **181**, 139–155 (2016).

58. Bonfim Santos, M. *et al.* Phylogenetic inferences reveal deep polyphyly of Aongstroemiaceae and Dicranellaceae within the haplolepideous mosses (Dicranidae, Bryophyta). *Taxon* **70**, 246–262 (2021).

59. Fedosov, V. E. *et al.* Unity in diversity: phylogenetics and taxonomy of

Rhabdoweisiaceae (Dicranales, Bryophyta). *Bot. J. Linn. Soc.* **195**, 545–567 (2021).

60. Budke, J., Jones, C. & Goffinet, B. Development of the enigmatic peristome of Timmia megapolitana (Timmiaceae; Bryophyta). *Am. J. Bot.* **94**, 460–467 (2007).

61. Rensing, S. A., Goffinet, B., Meyberg, R., Wu, S.-Z. & Bezanilla, M. The moss Physcomitrium (Physcomitrella) patens : A model organism for non-seed plants. *Plant Cell* **32**, 1361–1376 (2020).

62. Newton, A. E., Wikström, N., Bell, N., Forrest, L. L. & Ignatov, M. S. Dating the diversification of the pleurocarpous mosses. in *Pleurocarpous Mosses* (eds. Newton, A. E. & Tangney, R. S.) 337 (Systematics and Evolution, 2007).

63. Lloyd, G. T. *et al.* Dinosaurs and the Cretaceous Terrestrial Revolution. *Proc. R. Soc. B Biol. Sci.* **275**, 2483–2490 (2008).

64. Benton, M. J., Wilf, P. & Sauquet, H. The Angiosperm Terrestrial Revolution and the origins of modern biodiversity. *New Phytol.* **233**, 2017–2035 (2022).

65. Schuettpelz, E. & Pryer, K. M. Evidence for a Cenozoic radiation of ferns in an angiosperm-dominated canopy. *Proc. Natl. Acad. Sci.* **106**, 11200–11205 (2009).

66. Söderström, L. *et al.* World checklist of hornworts and liverworts. *PhytoKeys* **59**, 1–828 (2016).

67. Brinda, J. C. & Atwood, J. J. *Bryophyte nomenclator*. *Catalogue of life checklist*

(Jan 2023) (2023). doi:10.48580/dfqt-8zmp.

68. Goffinet, B. & Buck, W. R. Classification of the Bryophyta. *http://bryology. uconn. edu/classification/* (2020).

69. Doyle, J. & Doyle, J. A rapid DNA isolation procedure for small quantities of fresh leaf tissue. *Phytochem Bull.* **19**, 11–15 (1987).

70. Chang, Z. *et al.* Bridger: a new framework for de novo transcriptome assembly using RNA-seq data. *Genome Biol.* **16**, 30 (2015).

71. Junier, T. & Zdobnov, E. M. The Newick utilities: high-throughput phylogenetic tree processing in the Unix shell. *Bioinformatics* **26**, 1669–1670 (2010).

72. Larsson, A. AliView: a fast and lightweight alignment viewer and editor for large datasets. *Bioinformatics* **30**, 3276–3278 (2014).

73. Nguyen, L.-T., Schmidt, H., von Haeseler, A. & Minh, B. Q. IQ-TREE: A Fast and Effective Stochastic Algorithm for Estimating Maximum-Likelihood Phylogenies. *Mol. Biol. Evol.* **32**, 268–274 (2015).

74. Hoang, D. T., Chernomor, O., von Haeseler, A., Minh, B. Q. & Vinh, L. UFBoot2: Improving the Ultrafast Bootstrap Approximation. *Mol. Biol. Evol.* **35**, 518–522 (2017).

75. Zhang, C., Rabiee, M., Sayyari, E. & Mirarab, S. ASTRAL-III: polynomial time species tree reconstruction from partially resolved gene trees. *BMC Bioinformatics* **19**, 153 (2018).

76. Stamatakis, A. RAxML version 8: A tool for phylogenetic analysis and post-

analysis of large phylogenies. *Bioinformatics* **30**, 1312–1313 (2014).

77. Stamatakis, A. RAxML-VI-HPC: maximum likelihood-based phylogenetic analyses with thousands of taxa and mixed models. *Bioinformatics* **22**, 2688–2690 (2006).

78. Sayyari, E. & Mirarab, S. Fast Coalescent-Based Computation of Local Branch Support from Quartet Frequencies. *Mol. Biol. Evol.* **33**, 1654–1668 (2016).

79. Sayyari, E., Whitfield, J. B. & Mirarab, S. DiscoVista: Interpretable visualizations of gene tree discordance. *Mol. Phylogenet. Evol.* **122**, 110–115 (2018).

80. Cooper, B. J. *et al.* Target Enrichment and Extensive Population Sampling Help Untangle the Recent, Rapid Radiation of Oenothera Sect. Calylophus. *Syst. Biol.* **0**, 1–15 (2022).

81. Smith, S. & O'Meara, B. treePL: divergence time estimation using penalized likelihood for large phylogenies. *Bioinformatics* **28**, 2689–2690 (2012).

82. Maurin, K. J. L. An empirical guide for producing a dated phylogeny with treePL in a maximum likelihood framework. *arXiv* 2008.07054 (2020) doi:10.48550/arXiv.2008.07054.

83. Miller, M., Pfeiffer, W. & Schwartz, T. The CIPRES science gateway. in *Proceedings of the 2011 TeraGrid Conference: Extreme Digital Discovery* 1–8 (ACM, 2011). doi:10.1145/2016741.2016785.

84. Brown, J., Walker, J. & Smith, S. Phyx: phylogenetic tools for unix.

Bioinformatics **33**, 1886–1888 (2017).

85. Bouckaert, R. *et al.* Beast 2: a software platform for bayesian evolutionary analysis. *PLoS Comput. Biol.* **10**, e1003537 (2014).

86. Rambaut, A. FigTree-version 1.4. 3, a graphical viewer of phylogenetic trees. http://tree.bio.ed.ac.uk/software/figtree/. (2017).

87. Paradis, E. & Schliep, K. ape 5.0: an environment for modern phylogenetics and evolutionary analyses in R. *Bioinformatics* **35**, 526–528 (2019).

88. R Core Team, R. R: A language and environment for statistical computing. *Foundation for Statistical Computing* https://www.r-project.org/ (2020).

89. Werness, S. A. & Anderson, D. J. r8s, version 1.70 User's Manual. at (2004).

Table 1: Description of novel families and orders of liverworts and mosses.

MARCHANTIOPHYTA (LIVERWORTS)

Lejeuneales Bechteler, A.M. Sierra, D. Bell & D.G. Long ord. nov.

Leaves mostly 2-lobed, the ventral lobule forming a *Lejeunea*-type water sac, gynoecia with 1 archegonium and a single series of bracts and bracteoles, seta 4 cells in diameter, commonly articulate; Type: Lejeuneaceae Rostovzev, New Phytol. 9: 291. 1910; Lejeuneaceae.

Frullaniales D. Bell & D.G. Long ord. nov.

Leaves 3-lobed, the median lobule forming a *Frullania*-type water sac, underleaves bifid, gynoecia with multiple archegonia, bracts and bracteoles in 3 or 4 series, seta up to 12 cells in diameter, non-articulate; Type: Frullaniaceae Lorch in G.Lindau, Krypt.-Fl. Anf. 6: 174. 1914; Frullaniaceae.

Myliales D.G. Long & D. Bell ord. nov.

Leaves unlobed, branching mostly terminal, rhizoids numerous, leaves succubous, simple, gemmiferous, with reduced underleaves, dioicous, sporophyte enclosed in shoot calyptra and perianth; Type: Myliaceae Schljakov, Novosti Sist. Nizsh. Rast. 12: 308. 1975; Myliaceae.

BRYOPHYTA (MOSSES)

Amphidiales D. Bell & Goffinet ord. nov.

Plants acrocarpous, forming dense cushions, leaves crisped when dry, capsules gymnostomous, emergent to shortly exserted; Type: Amphidiaceae M. Stech, Nova Hedwigia 86: 14, 2008; Amphidiaceae.

Bruchiales Goffinet ord. nov.

Plants erect, acrocarpous, capsule with well-developed neck, peristome haplolepideous; Type: Bruchiaceae Schimp., Coroll. Bryol. Eur.: 6, 1856; Bruchiaceae.

Distichiales D. Bell & Goffinet ord. nov.

Plants acrocarpous, leaves distichous, spreading from broad sheathing base, costa excurrent, monoecious, peristome haplolepideous; Type: Distichiaceae Schimp., Syn. Musc. Eur. 135. 1860; Distichiaceae.

Ditrichales D. Bell & Goffinet ord. nov.

Plants erect, acrocarpous, with costate and mostly lanceolate leaves, sporangium exserted with haplolepideous peristome, or immersed and cleistocarpous. Type: Ditrichaceae Limpr., Laubm. Deutschl. 1: 482, 1887; Ditrichaceae.

Erpodiales Goffinet ord. nov.

Plants small, plagiotropic, leaves ecostate, cladocarpous, peristome haplolepideous; Type: Erpodiaceae Broth., Nat. Pflanzenfam. I(3): 706. 1905; Erpodiaceae.

Eustichiales Goffinet ord. nov.

Plants erect, leaves single costate, distichous with sheathing laminae, with lateral sporophytes and erect capsules; Type: Eustichiaceae Broth., Nat. Pflanzenfam. (ed. 2) 10: 420, 1924; Eustichiaceae.

Flexitrichaceae Ignatov & Fedosov ex Goffinet fam. nov. for Flexitrichaceae Ignatov & Fedosov invalid

Plants acrocarpous; leaves straight to flexuose, from sheathing bases, dioecious, peristome haplolepideous; Type: *Flexitrichum* Ignatov & Fedosov, Bot. J. Linn. Soc. 181(2): 152. 2016; *Flexitrichum*.

Flexitrichales D. Bell & Goffinet ord. nov.

Plants acrocarpous; leaves straight to flexuose, from sheathing bases, dioecious; Type: Flexitrichaceae Ignatov & Fedosov ex D. Bell & Goffinet; Flexitrichaceae.

Pleurophascales Goffinet ord. nov.

Plants robust, stems plagiotropic, branches erect, leaves acostate, sporophyte exserted, capsule globose, cleistocarpous; Type: Pleurophascaceae Broth. Nat. Pflanzenfam. I(3): 774, 1906; Pleurophascaceae.

Rhabdoweisiales D. Bell & Goffinet ord. nov.

Plants small, erect, acrocarpous, leaves unicostate, unistratose, peristome haplolepideous; Type: Rhabdoweisiaceae Limpr. Laubm. Deutschl. 1: 271, 1886; Rhabdoweisiaceae[52] and Rhachitheciaceae.

Sorapillales Goffinet ord. nov.

Plants monopodial, vaginant leaves distichous, complanate, sporophyte lateral, immersed, peristome haplolepideous with vestigial exostome; Type: Sorapillaceae M. Fleisch, Musci Buitenzorg 3: 847, 1908; Sorapillaceae.

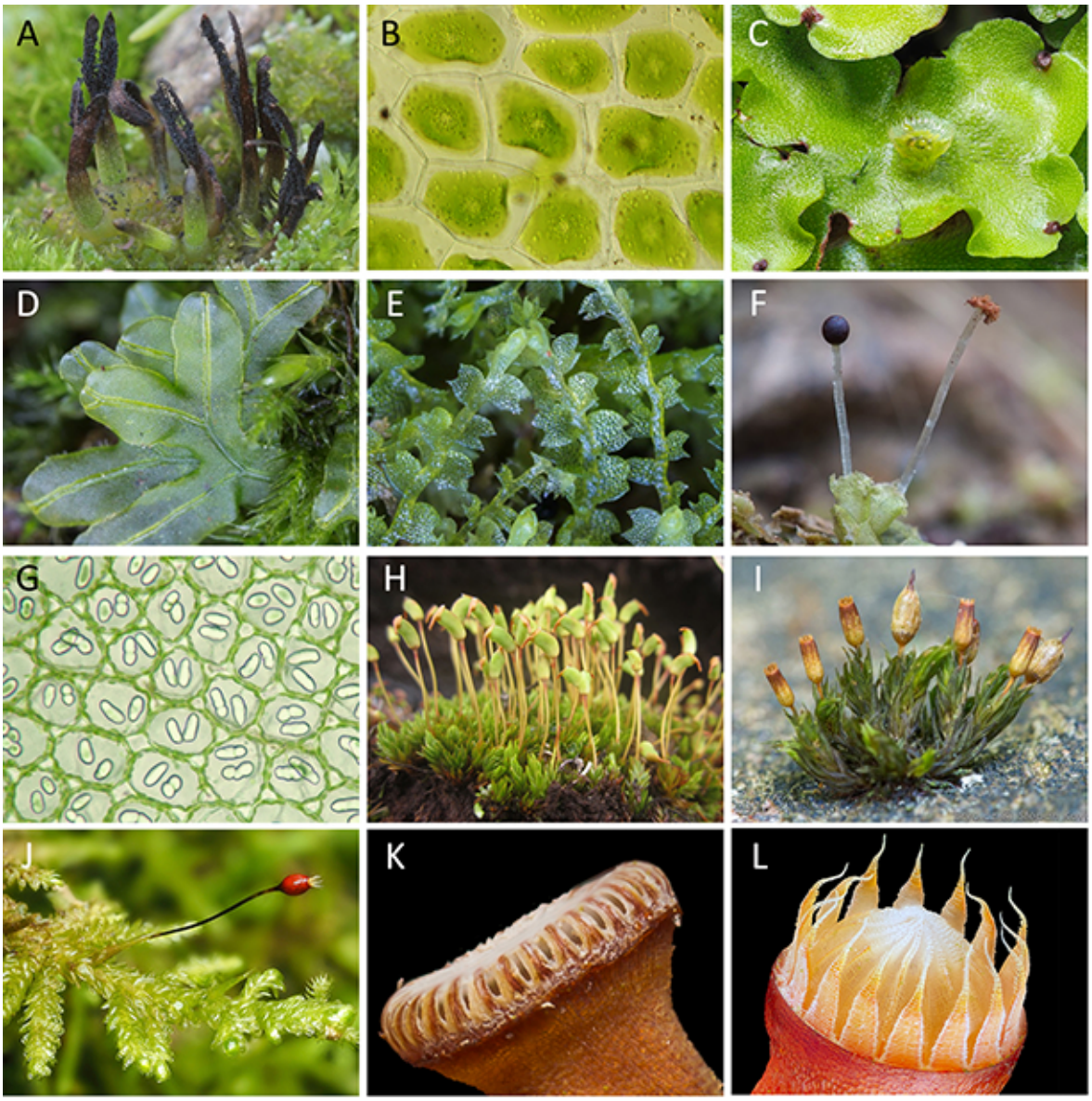

Figure 1. Representatives of major lineages of bryophytes and examples of traits unique to hornworts, liverworts and mosses. A. Hornwort with longitudinally dehiscing sporophyte: *Anthoceros neesii*. B. Pyrenoid (arrowheads) of the hornwort *Phaeoceros perpusillus*. C. Complex thalloid liverwort: *Marchantia paleacea*. D. Simple thalloid liverwort: *Metzgeria conjugata*. E. Leafy liverwort: *Leiocolea badensis*. F. Liverwort sporophyte before (left) and after (right) dehiscence: *Fossombronia pusilla*. G. Oil bodies of *Gymnocolea inflata*. H. Polytrichopsida moss: *Atrichopsis trichodon.* I. Acrocarpous moss: *Orthotrichum anomalum*. J. Pleurocarpous moss: *Exsertotheca intermedia.* K. Nematodontous peristome of *Polytrichum ohioense*. L. Arthrodontous peristome of *Bryum capillare*. Pictures kindly shared by Štěpán Koval (A, D, E, F & I), Sahut Chantanaorrapint (B), Des Callaghan (C, J & L), Bernard Goffinet (H), Jerry Jenkins (K) and David Wagner (G).

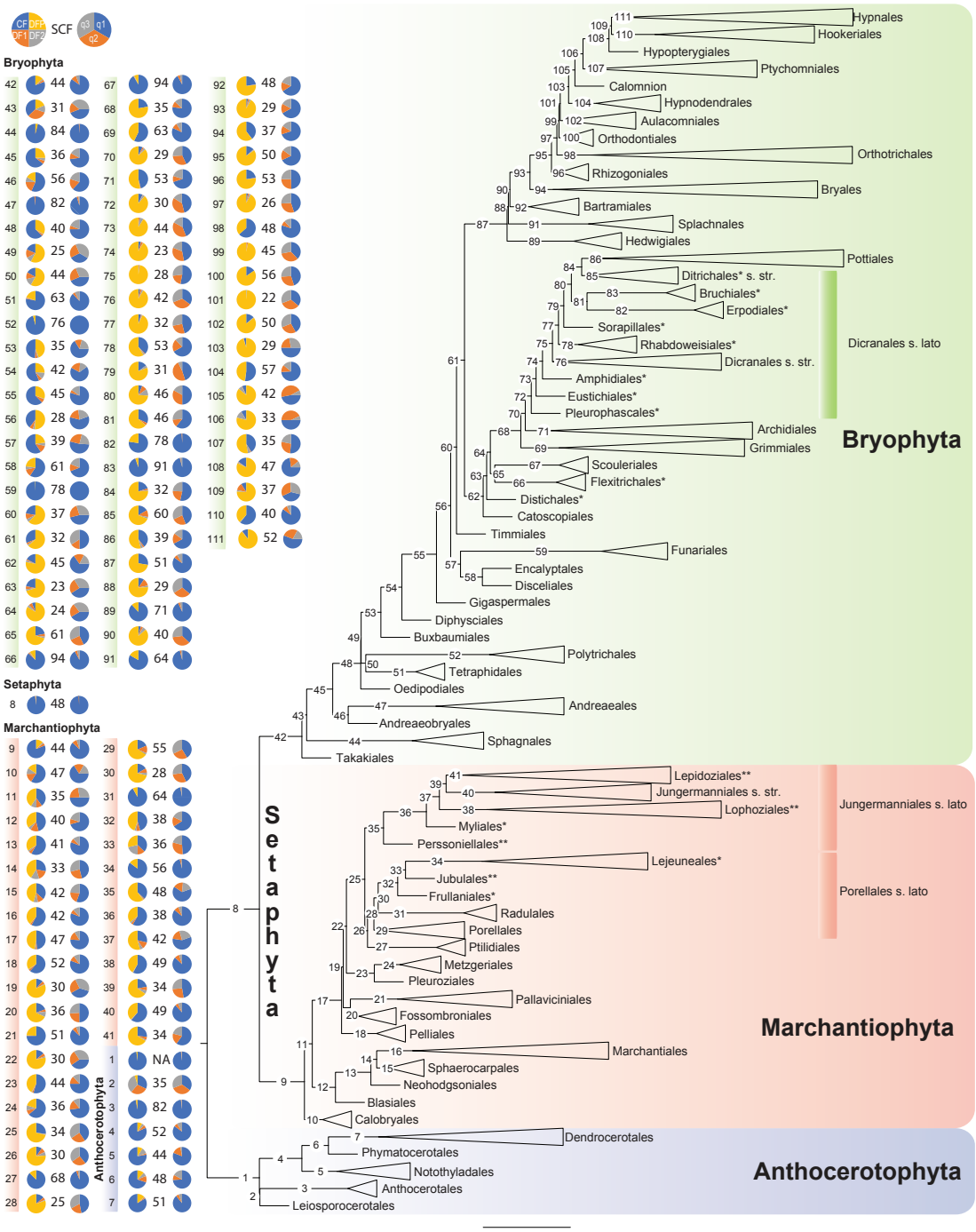

Figure 2. Phylogenetic inferences for 531 species from 499 genera belonging to orders from all three bryophyte groups (mosses, liverworts and hornworts) based on ASTRAL analysis of 228 single-copy nuclear genes (Supplementary Tables S1 and S3). The phylogram shows internal branch lengths relative to coalescent unites between branching events, as estimated by ASTRAL-III v.5.7.7. The nodes of interests have been numbered to illustrate quartet values from ASTRAL analyses presented as pie-charts (right) and quartet values from concordance factor values (left), while the number in the center is the site concordance factor (sCF). ASTRAL pies are divided into q1 (blue), q2 (orange) and q3 (grey) with the percentage for q1 included in the pie diagram; see Supplementary Fig. S1 and Fig. S2 for quartet values for all other nodes and local posterior probabilities. Pies for quartet values from concordance factor values: CF (topology shown) and alternative options (DF1, DF2, DFP); see Supplementary Tables S4-S6 for the concordance factors for all nodes. * marks newly proposed order and ** resurrected order.

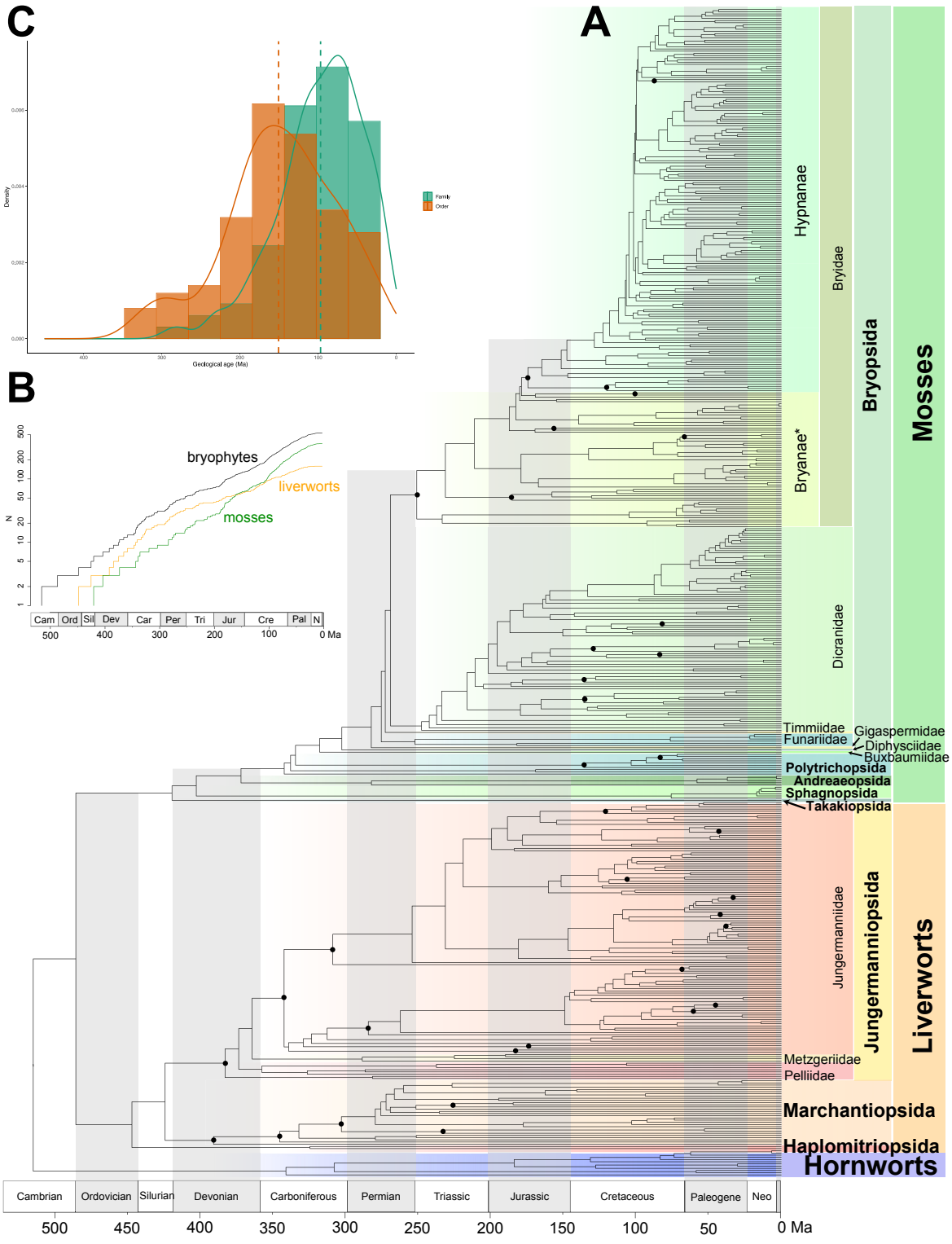

Figure 3. A. Divergence time estimates for bryophytes inferred by penalized likelihood using 29 fossil calibrations. The three bryophyte groups (hornworts, liverworts, mosses) are included with their major suprafamilial taxonomic ranks including classes, subclasses, orders and suborders. Black dots scattered in the tree represent calibration points (Supplementary Table S2). Detailed chronograms with mean node ages including confidence intervals are reported in three parts: liverworts and hornworts in Extended Data Figure 7-1, mosses Extended Data Figure 7-2 and Extended Data Figure 7-3. **B**. Lineage through time plots of all bryophytes (black line), liverworts (orange line) and mosses (green line), reflecting the slowdown in diversification in liverworts during the Late Cretaceous when

compared to mosses. **C**. Histogram of the frequency of orders and families estimated from crown age divergences of all bryophytes (hornworts, liverworts, and mosses). Kernel density plots depict the probability distribution (95% confidence interval) of crown age divergences. The green dotted line represents the average of family crown ages and orange dotted line represents the average of order crown ages. See also Extended Data Fig. 10, Supplementary Table S10 and Supplementary Fig. S9.

Extended data

Phylogenomic time tree of bryophytes resolves 500 million years of diversification

Table of content

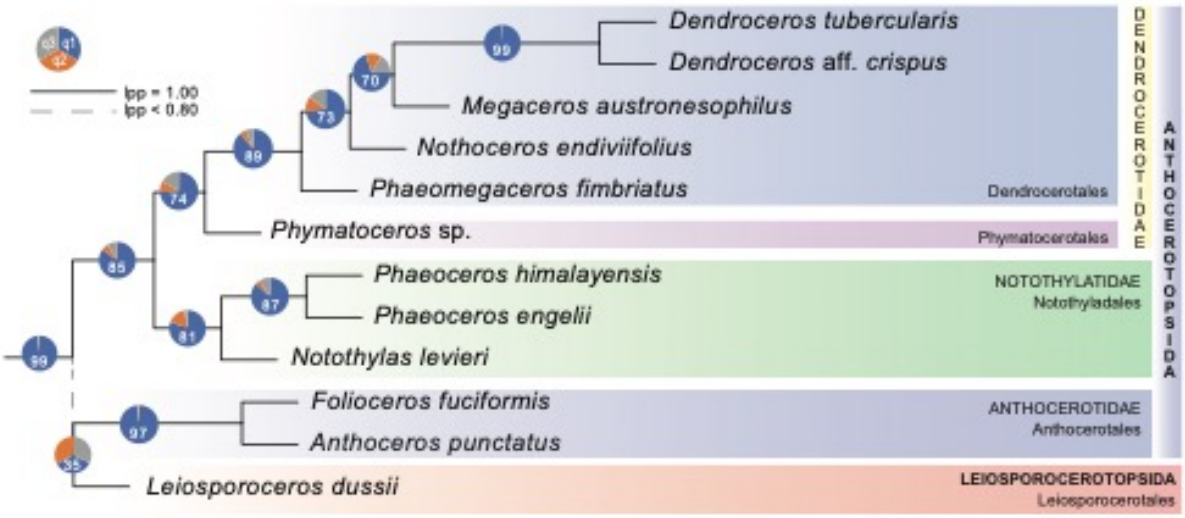

Extended Data Figure 1. Annotated ASTRAL phylogeny of hornworts inferred from nucleotide data, highlighting (supra-)ordinal relationships. Quartet values from ASTRAL analyses are presented as pie-charts (q1:blue; q2:orange; q3:grey) for selected nodes with the percentage for the first quartet (q1) included in the pie diagram; see Fig. S1 for quartet values for all other nodes. Branches with maximum local posterior probability (lpp) are represented as solid black lines; those with a lpp below 0.80 as a grey dashed line; see Fig. S2 for detailed lpp for all branches.

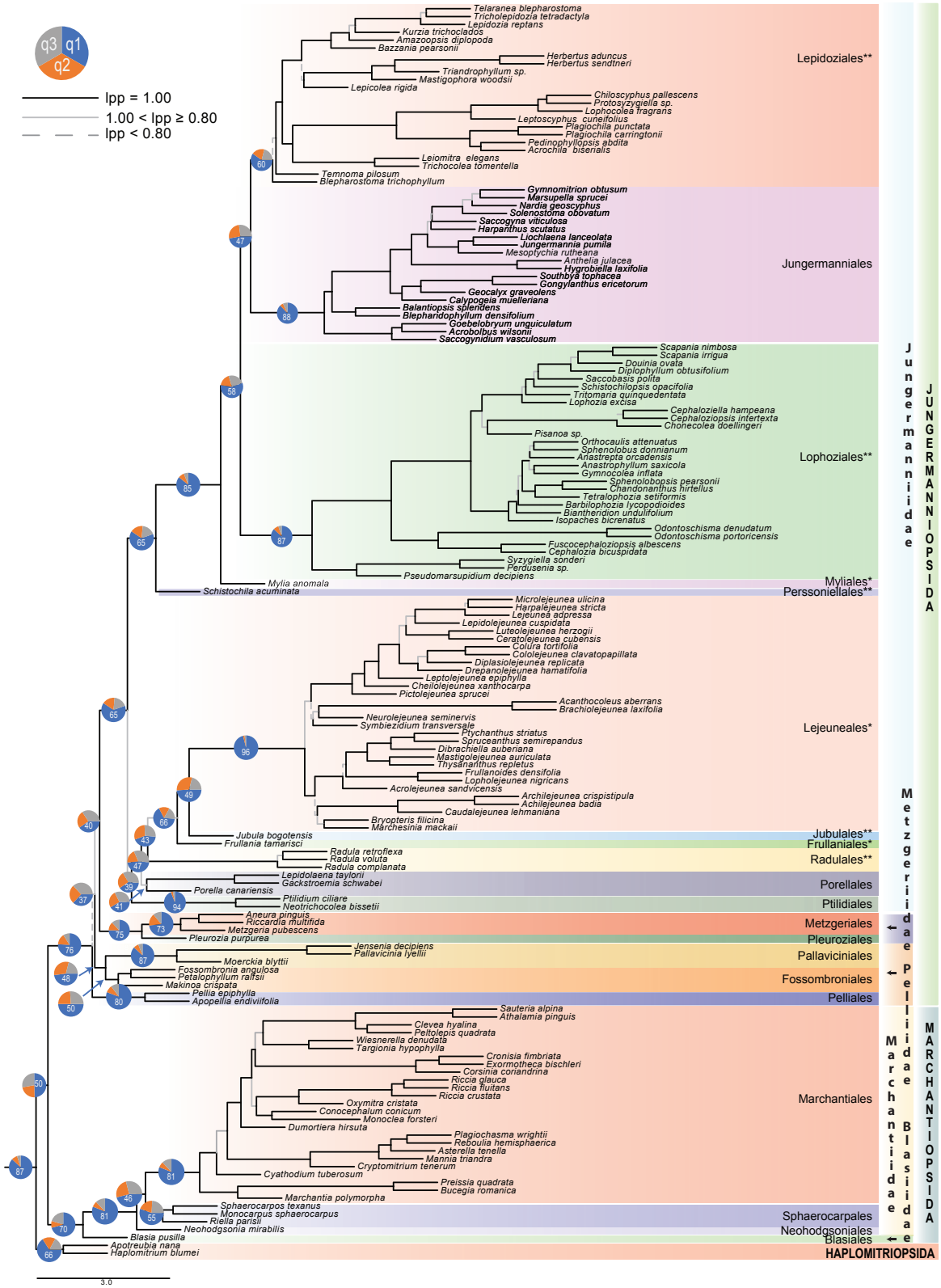
q3
q1
q2
lpp = 1.00
1.00 < lpp ≥ 0.80
lpp < 0.80
Telaranea blepharostoma
Tricholepidozia tetradactyla
Lepidozia reptans
Kurzia trichoclados
Amazoopsis diplopoda
Bazzania pearsonii
Herbertus aduncus
Herbertus sendtneri
Triandrophyllum sp.
Mastigophora woodsii
Lepicolea rigida
Chiloscyphus pallescens
Protosyzygiella sp.
Lophocolea fragrans
Leptoscyphus cuneifolius
Plagiochila punctata
Plagiochila carringtonii
Pedinophyllopsis abdita
Acrochila biserialis
Leiomitra elegans
Trichocolea tomentella
Temnoma pilosum
Blepharostoma trichophyllum
Lepidoziales**
Gymnomitrion obtusum
Marsupella sprucei
Nardia geoscyphus
Solenostoma obovatum
Saccogyna viticulosa
Harpanthus scutatus
Liochlaena lanceolata
Jungermannia pumila
Mesoptychia rutheana
Anthelia julacea
Hygrobiella laxifolia
Southbya tophacea
Gongylanthus ericetorum
Geocalyx graveolens
Calypogeia muelleriana
Balantiopsis splendens
Blepharidophyllum densifolium
Goebelobryum unguiculatum
Acrobolbus wilsonii
Saccogynidium vasculosum
Jungermanniales
Scapania nimbosa
Scapania irrigua
Douinia ovata
Diplophyllum obtusifolium
Saccobasis polita
Schistochilopsis opacifolia
Tritomaria quinquedentata
Lophozia excisa
Cephaloziella hampeana
Cephaloziopsis intertexta
Chonecolea doellingeri
Pisanoa sp.
Orthocaulis attenuatus
Sphenolobus donnianum
Anastrepta orcadensis
Anastrophyllum saxicola
Gymnocolea inflata
Sphenolobopsis pearsonii
Chandonanthus hirtellus
Tetralophozia setiformis
Barbilophozia lycopodioides
Biantheridion undulifolium
Isopaches bicrenatus
Odontoschisma denudatum
Odontoschisma portoricensis
Fuscocephaloziopsis albescens
Cephalozia bicuspidata
Syzygiella sonderi
Perdusenia sp.
Pseudomarsupidium decipiens
Lophoziales**
Mylia anomala
Myliales*
Schistochila acuminata
Perssoniellales**
Jungermanniidae
JUNGERMANNIOPSIDA
Microlejeunea ulicina
Harpalejeunea stricta
Lejeunea adpressa
Lepidolejeunea cuspidata
Luteolejeunea herzogii
Ceratolejeunea cubensis
Colura tortifolia
Cololejeunea clavatopapillata
Diplasiolejeunea replicata
Drepanolejeunea hamatifolia
Leptolejeunea epiphylla
Cheilolejeunea xanthocarpa
Pictolejeunea sprucei
Acanthocoleus aberrans
Brachiolejeunea laxifolia
Neurolejeunea seminervis
Symbiezidium transversale
Ptychanthus striatus
Spruceanthus semirepandus
Dibrachiella auberiana
Mastigolejeunea auriculata
Thysananthus repletus
Frullanoides densifolia
Lopholejeunea nigricans
Acrolejeunea sandvicensis
Archilejeunea crispistipula
Achilejeunea badia
Caudalejeunea lehmaniana
Bryopteris filicina
Marchesinia mackaii
Lejeuneales*
Jubula bogotensis
Jubulales**
Frullania tamarisci
Frullaniales*
Radula retroflexa
Radula voluta
Radula complanata
Radulales**
Lepidolaena taylorii
Gackstroemia schwabei
Porellales
Porella canariensis
Ptilidium ciliare
Neotrichocolea bissetii
Ptilidiales
Aneura pinguis
Riccardia multifida
Metzgeria pubescens
Metzgeriales
Pleurozia purpurea
Pleurozioles
Jensenia decipiens
Pallavicinia lyellii
Pallaviciniales
Moerckia blyttii
Fossombronia angulosa
Petalophyllum ralfsii
Makinoa crispata
Fossombroniales
Pellia epiphylla
Apopellia endiviifolia
Pelliales
Metzgeriidae
Pelliidae
Sauteria alpina
Athalamia pinguis
Clevea hyalina
Peltolepis quadrata
Wiesnerella denudata
Targionia hypophylla
Cronisia fimbriata
Exormotheca bischleri
Corsinia coriandrina
Riccia glauca
Riccia fluitans
Riccia crustata
Oxymitra cristata
Conocephalum conicum
Monoclea forsteri
Dumortiera hirsuta
Plagiochasma wrightii
Reboulia hemisphaerica
Asterella tenella
Mannia triandra
Cryptomitrium tenerum
Cyathodium tuberosum
Preissia quadrata
Bucegia romanica
Marchantia polymorpha
Marchantiales
Sphaerocarpos texanus
Monocarpus sphaerocarpus
Riella parisii
Sphaerocarpales
Neohodgsonia mirabilis
Neohodgsoniales
Blasia pusilla
Blasiales
Apotreubia nana
Haplomitrium blumei
HAPLOMITRIOPSIDA
Marchantiidae
Blasiidae
MARCHANTIOPSIDA
3.0

Extended Data Figure 2. Annotated ASTRAL phylogeny of liverworts inferred from nucleotide data, highlighting suprafamilial relationships. Quartet values from ASTRAL analyses are presented as pie-charts (q1:blue; q2:orange; q3:grey) for selected nodes with the percentage for the first quartet (q1) included in the pie diagram; see Fig. S1 for quartet values for all other nodes. Branches with maximum local posterior probability (lpp) are represented as solid black lines; those with a lpp between 0.8 and 1.0 as a solid grey line and those with a lpp below 0.80 as a grey dashed line; see Fig. S2 for detailed lpp for all branches. Asterisk marks novel order, and double Asterisk resurrected order.

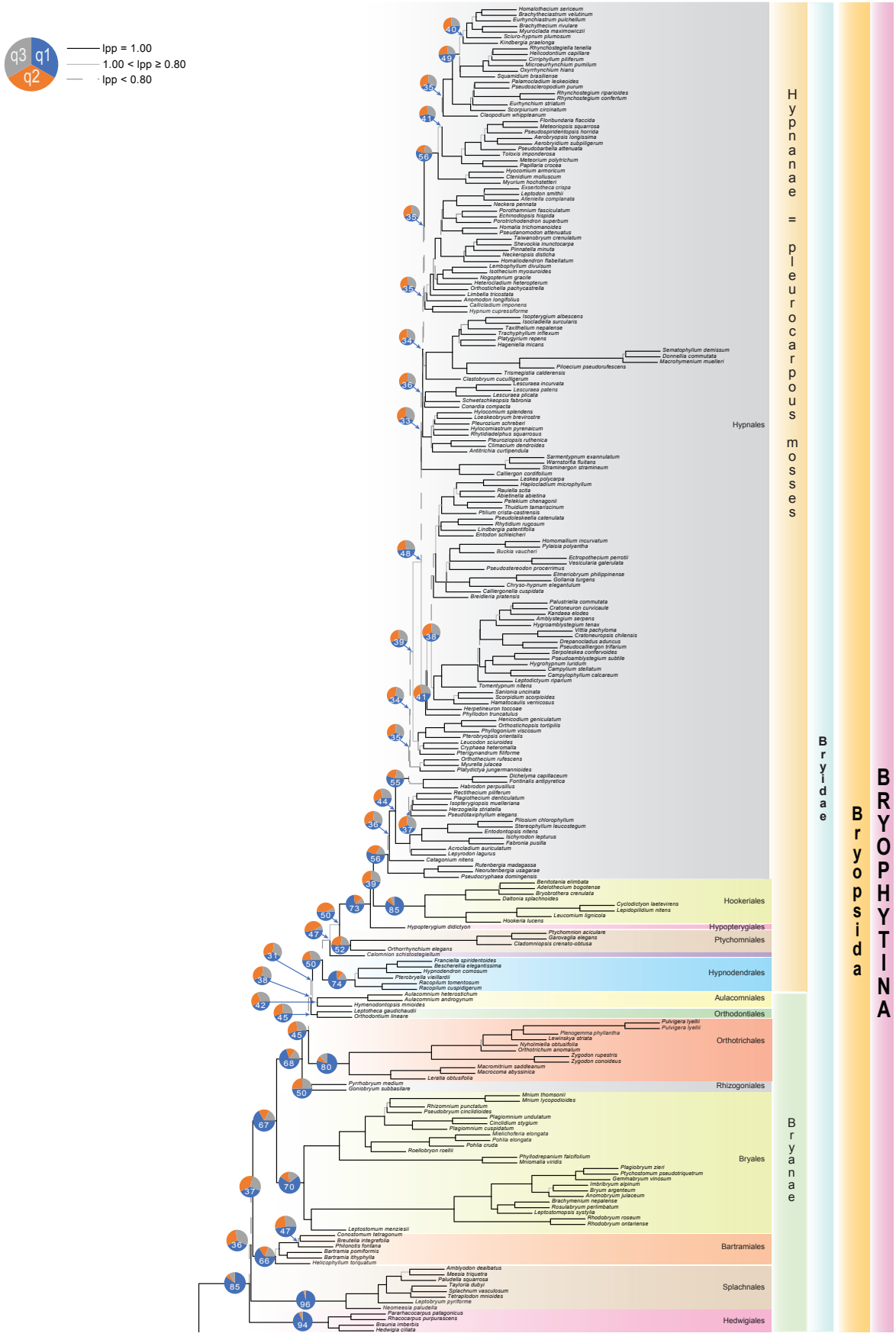
q3
q1
q2
lpp = 1.00
1.00 < lpp ≥ 0.80
lpp < 0.80
Homalothecium sericeum
Brachytheciastrum velutinum
Eurhynchiastrum pulchellum
Brachythecium rivulare
Myuroclada maximowiczii
Sciuro-hypnum plumosum
Kindbergia praelonga
Rhynchostegiella tenella
Helicodontium capillare
Cirriphyllum piliferum
Microeurhynchium pumilum
Oxyrrhynchium hians
Squamidium brasiliense
Palamocladium leskeoides
Pseudoscleropodium purum
Rhynchostegium riparioides
Rhynchostegium confertum
Eurhynchium striatum
Scorpiurium circinatum
Claopodium whippleanum
Floribundaria flaccida
Meteoriopsis squarrosa
Pseudospiridentopsis horrida
Aerobryopsis longissima
Aerobryidium subpiligerum
Pseudobarbella attenuata
Toloxis imponderosa
Meteorium polytrichum
Papillaria crocea
Hyocomium armoricum
Ctenidium molluscum
Myurium hochstetteri
Exsertotheca crispa
Leptodon smithii
Alleniella complanata
Neckera pennata
Porothamnium fasciculatum
Echinodiopsis hispida
Porotrichodendron superbum
Homalia trichomanoides
Pseudanomodon attenuatus
Taiwanobryum crenulatum
Shevockia inunctocarpa
Pinnatella minuta
Neckeropsis disticha
Homaliodendron flabellatum
Lembophyllum divulsum
Isothecium myosuroides
Ningpoterium gracile
Heterocladium heteropterum
Orthostichella pachycastrella
Limbella tricostata
Anomodon longifolius
Callicladium imponens
Hypnum cupressiforme
Hypnales
Hypopterygium albescens
Isocladiella surcularis
Taxithelium nepalense
Trachyphyllum inflexum
Platygyrium repens
Hageniella micans
Sematophyllum demissum
Donnellia commutata
Macrohymenium muelleri
Pilocium pseudorufescens
Trismegistia calderensis
Clastobryum cuculligerum
Lescuraea incurvata
Lescuraea patens
Lescuraea plicata
Schwetschkeopsis fabronia
Conardia compacta
Hylocomium splendens
Loeskeobryum brevirostre
Pleurozium schreberi
Hylocomiastrum pyrenaicum
Rhytidiadelphus squarrosus
Pleuroziopsis ruthenica
Climacium dendroides
Antitrichia curtipendula
Sarmentypnum exannulatum
Warnstorfia fluitans
Straminergon stramineum
Calliergon cordifolium
Leskea polycarpa
Haplocladium microphyllum
Rauiella scita
Abietinella abietina
Pelekium chenagonii
Thuidium tamariscinum
Ptilium crista-castrensis
Pseudoleskeella catenulata
Rhytidium rugosum
Lindbergia paternifolia
Entodon schleicheri
Homomallium incurvatum
Pylaisia polyantha
Buckia vaucheri
Ectropothecium perrotii
Vesicularia galeriulata
Pseudostereodon procerrimus
Elmeriobryum philippinense
Gollania turgens
Chryso-hypnum elegantulum
Calliergonella cuspidata
Breidleria pratensis
Palustriella commutata
Cratoneuron curvicaule
Kandaea elodes
Amblystegium serpens
Hygroamblystegium tenax
Vittia pachyloma
Crateroneuropsis chilensis
Drepanocladus aduncus
Pseudocalliergon trifarium
Serpoleskea confervoides
Pseudoamblystegium subtile
Hygrohypnum luridum
Campylium stellatum
Campylophyllum calcareum
Leptodictyum riparium
Tomentypnum nitens
Sanionia uncinata
Scorpidium scorpioides
Hamatocaulis vernicosus
Herpetineuron toccoae
Phyllodon truncatulus
Henicodium geniculatum
Orthostichopsis tortipilis
Phyllogonium viscosum
Pterobryopsis orientalis
Leucodon sciuroides
Cryphaea heteromalla
Pterigynandrum filiformne
Orthothecium rufescens
Myurella julacea
Platydictya jungermannioides
Dichelyma capillaceum
Fontinalis antipyretica
Habrodon perpusillus
Rectithecium piliferum
Plagiothecium denticulatum
Isopterygiopsis muelleriana
Herzogiella striatella
Pseudotaxiphyllum elegans
Pilosium chlorophyllum
Stereophyllum leucostegum
Entodontopsis nitens
Ischyrodon lepturus
Fabronia pusilla
Acrocladium auriculatum
Lepyrodon lagurus
Catagonium nitens
Rutenbergia madagassa
Neorutenbergia usagarae
Pseudocryphaea domingensis
Benitotania elimbata
Adelothecium bogotense
Brybrothera crenulata
Daltonia splachnoides
Cyclodictyon laetevirens
Lepidopilidium nitens
Leucomium lignicola
Hookeria lucens
Hookeriales
Hypopterygium didictyon
Hypopterygiales
Ptychomnion aciculare
Garovaglia elegans
Cladomniopsis crenato-obtusa
Ptychomniales
Orthorrhynchium elegans
Calomnion schistostegieillum
Franciella spiridentoides
Bescherella elegantissima
Hypnodendron comosum
Pterobryella vieillardii
Racopilum tomentosum
Racopilum cuspidigerum
Hypnodendrales
Aulacomnium heterostichum
Aulacomnium androgynum
Aulacomniales
Hymenodontopsis mnioides
Leptotheca gaudichaudii
Orthodontium lineare
Orthodontiales
Pulvigera lyellii
Pulvigera lyellii
Plenogemma phyllantha
Lewinskya striata
Nyholmiella obtusifolia
Orthotrichum anomalum
Zygodon rupestris
Zygodon conoideus
Macromitrium saddleanum
Macrocoma abyssinica
Leratia obtusifolia
Orthotrichales
Pyrrhobryum medium
Goniobryum subbasilare
Rhizogoniales
Mnium thomsonii
Mnium lycopodioides
Rhizomnium punctatum
Pseudobryum cinclidioides
Plagiomnium undulatum
Cinclidium stygium
Plagiomnium cuspidatum
Mielichoferia elongata
Pohlia elongata
Pohlia cruda
Roellobryon roellii
Phyllodrepanium falcifolium
Mniomalia viridis
Plagiobryum zieri
Ptychostomum pseudotriquetrum
Gemmabryum vinosum
Imbribryum alpinum
Bryum argenteum
Anomobryum julaceum
Brachymenium nepalense
Rosulabryum perlimbatum
Leptostomopsis systylia
Rhodobryum roseum
Rhodobryum ontariense
Bryales
Leptostomum menziesii
Conostomum tetragonum
Breutelia integrifolia
Philonotis fontana
Bartramia pomiformis
Bartramia thyphylla
Helicophyllum torquatum
Bartramiales
Amblyodon dealbatus
Meesia triquetra
Paludella squarrosa
Tayloria dubyi
Splachnum vasculosum
Tetraplodon mnioides
Leptobryum pyriforme
Splachnales
Neomeesia paludella
Parahaocarpus patagonicus
Rhacocarpus purpurascens
Brauna imberbis
Hedwigia ciliata
Hedwigiales
Hypnanae = pleurocarpous mosses
Bryidae
Bryopsida
BRYOPHYTINA
Bryanae

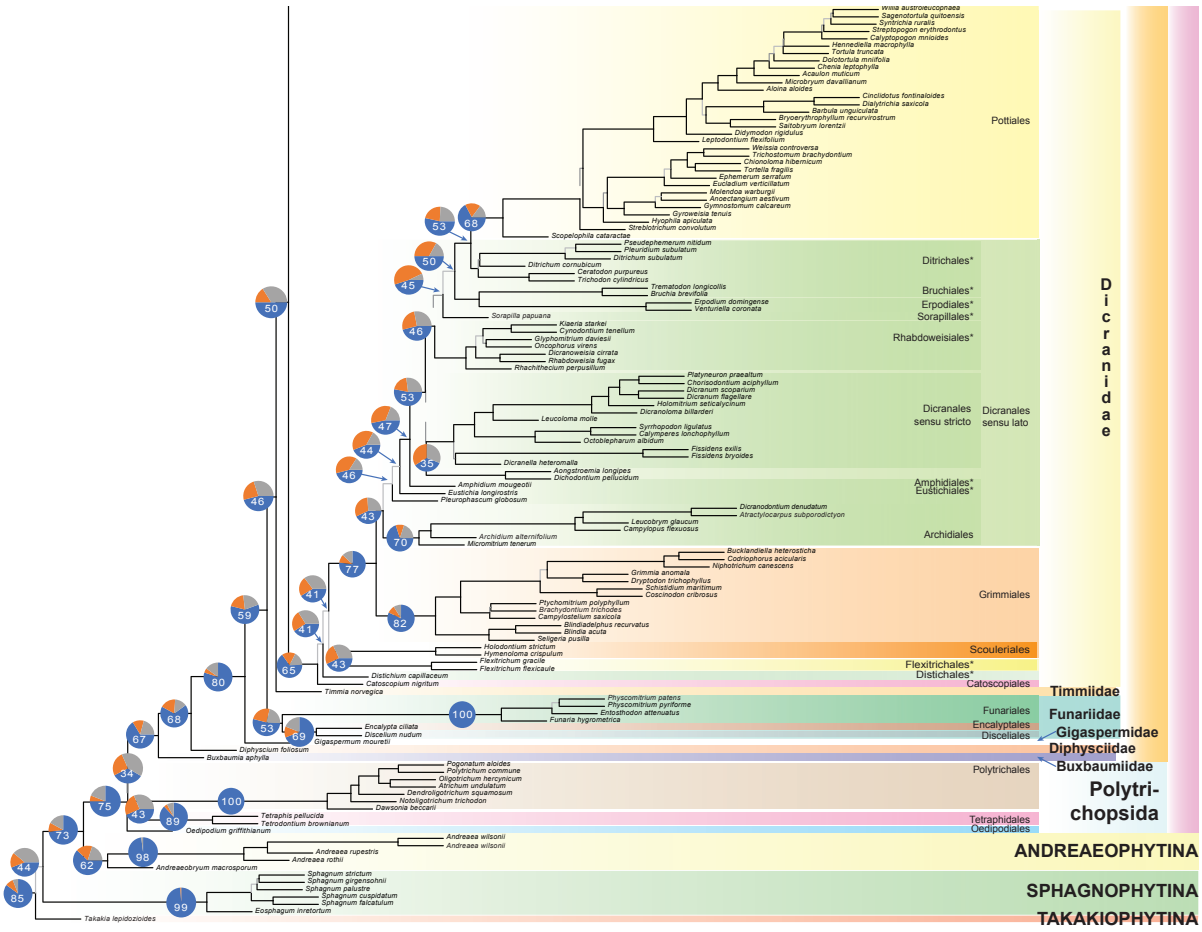

Extended Data Figure 3. Annotated ASTRAL phylogeny of mosses inferred from nucleotide data, highlighting suprafamilial relationships. Quartet values from ASTRAL analyses are presented as pie-charts (q1:blue; q2:orange; q3:grey) for selected nodes with the percentage for the first quartet (q1) included in the pie diagram; see Fig. S1 for quartet values for all other nodes. Branches with maximum local posterior probability (lpp) are represented as solid black lines; those with a lpp between 0.8 and 1.0 as a solid grey line and those with a lpp below 0.80 as a grey dashed line; see Fig. S2 for detailed lpp for all branches. Asterisks mark novel orders.

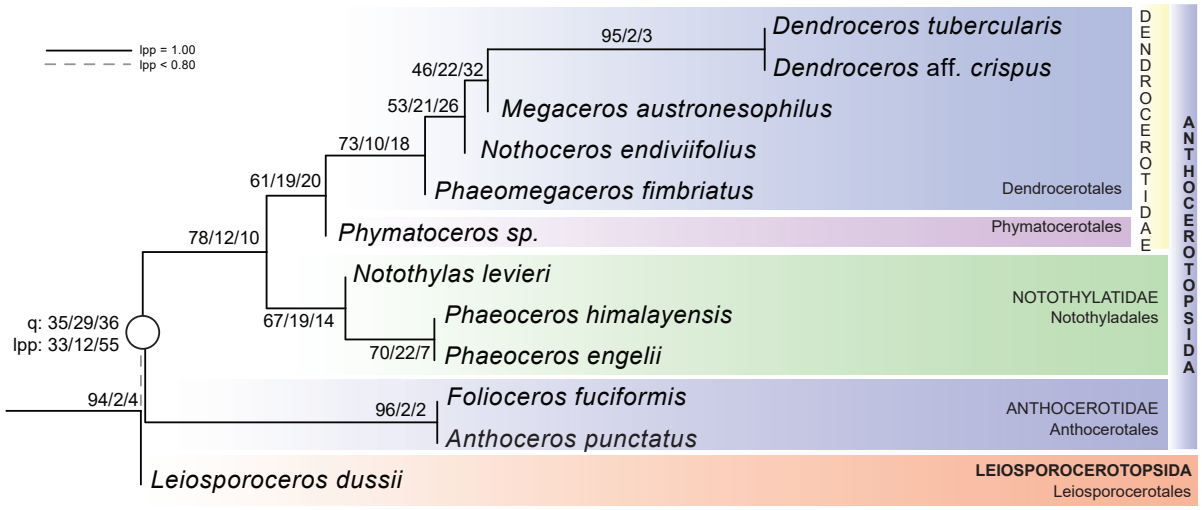

Extended Data Figure 4. Annotated ASTRAL phylogeny of hornworts inferred from amino acid data, highlighting (supra)ordinal relationships. Quartet values for the three possible topologies are presented as percentages near the node. Branches with maximum local posterior probability (lpp) are represented as solid black lines; those with a lpp below 0.80 as a grey dashed line; see Fig. S7 for detailed lpp for all branches.

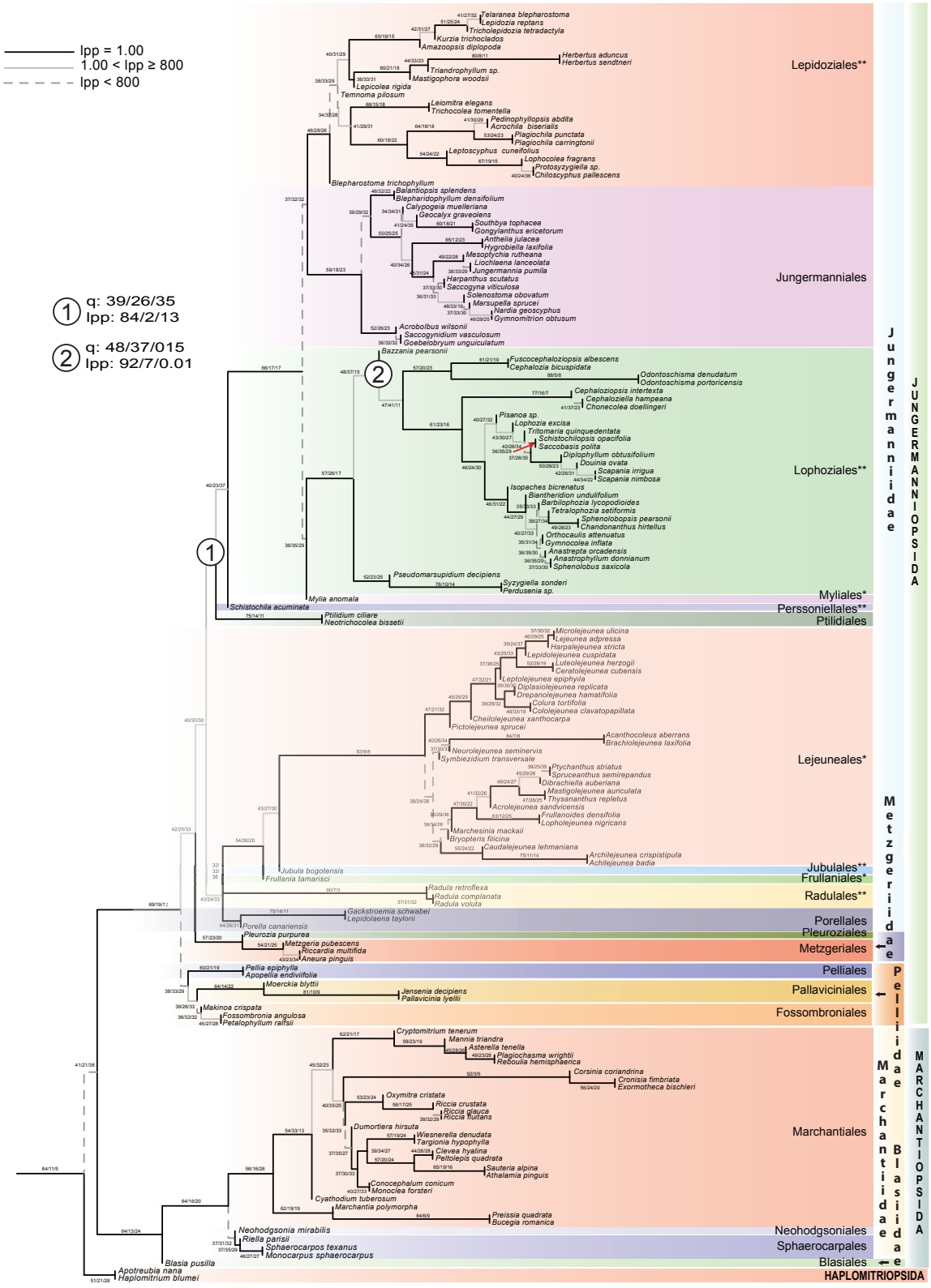
lpp = 1.00
1.00 < lpp ≥ 800
lpp < 800
① q: 39/26/35 lpp: 84/2/13
② q: 48/37/015 lpp: 92/7/0.01
Telaranea blepharostoma
Lepidozia reptans
Tricholepidozia tetradactyla
Kurzia trichoclados
Amazoopsis diplopoda
Herbertus aduncus
Herbertus sendtneri
Triandrophyllum sp.
Mastigophora woodsii
Lepicolea rigida
Temnoma pilosum
Leiomitra elegans
Trichocolea tomentella
Pedinophyllopsis abdita
Acrochila biserialis
Plagiochila punctata
Plagiochila carringtonii
Leptoscyphus cuneifolius
Lophocolea fragrans
Protosyzygiella sp.
Chiloscyphus pallescens
Blepharostoma trichophyllum
Lepidoziales**
Balantiopsis splendens
Blepharidophyllum densifolium
Calypogeia muelleriana
Geocalyx graveolens
Southbya tophacea
Gongylanthus ericetorum
Anthelia juracea
Hygrobiella laxifolia
Mesoptychia rutheana
Lophozia excisa
Lochlaena lanceolata
Jungermannia pumila
Harpanthus scutatus
Saccogyna viticulosa
Solenostoma obovatum
Marsupella sprucei
Nardia geoscyphus
Gymnomitrion obtusum
Acrobolbus wilsonii
Saccogynidium vasculosum
Goebelobryum unguiculatum
Jungermanniales
Bazzania pearsonii
Fuscocephaloziopsis albescens
Cephalozia bicuspidata
Odontoschisma denudatum
Odontoschisma portoricensis
Cephaloziopsis intertexta
Cephalozia hampeana
Chonecolea doellingeri
Pisanoa sp.
Tritomaria quinquedentata
Schistochilopsis opacifolia
Saccobasis polita
Diplophyllum obtusifolium
Douinia ovata
Scapania irrigua
Scapania nimbosa
Isopaches bicrenatus
Blantheridion undulifolium
Barbilophozia lycopodioides
Tetralophozia setiformis
Sphenolobopsis pearsonii
Chandonanthus hirtellus
Orthocaulis attenuatus
Gymnocolea inflata
Anastrepta orcadensis
Anastrophyllum donnianum
Sphenolobus saxicola
Lophoziales**
Pseudomarsupidium decipiens
Syzygiella sonderi
Perdusenia sp.
Mylia anomala
Myliales*
Schistochila acuminata
Perssoniellales**
Ptilidium ciliare
Neotrichocolea bissetii
Ptilidiales
Jungermanniidae
JUNGERMANNIOPSIDA
Microlejeunea ulicina
Lejeunea adpressa
Harpalejeunea stricta
Lepidolejeunea cuspidata
Luteolejeunea herzogii
Ceratolejeunea cubensis
Leptolejeunea epiphyla
Diplasiolejeunea replicata
Drepanolejeunea hamatifolia
Colura tortifolia
Cololejeunea clavatopapillata
Cheilolejeunea xanthocarpa
Pictolejeunea sprucei
Acanthocoleus aberrans
Brachiolejeunea laxifolia
Neurolejeunea seminervis
Symbiezidium transversale
Ptychanthus striatus
Spruceanthus semirepandus
Dibrachiella auberiana
Mastigolejeunea auriculata
Thysananthus repletus
Acrolejeunea sandvicensis
Frullanoides densifolia
Lopholejeunea nigricans
Marchesinia mackaii
Bryopteris filicina
Caudalejeunea lehmaniana
Archilejeunea crispistipula
Archilejeunea badia
Lejeuneales*
Jubula bogotensis
Frullania tamarisci
Jubulales**
Frullaniales*
Radula retroflexa
Radula complanata
Radula voluta
Radulales**
Gackstroemia schwabei
Lepidolaena taylorii
Porella canariensis
Porellales
Pleurozia purpurea
Pleuroziales
Metzgeria pubescens
Riccardia multifida
Aneura pinguis
Metzgeriales
Metzgeriidae
Pellia epiphylla
Apopellia endiviifolia
Pelliales
Moerckia blyttii
Jensenia decipiens
Pallavicinia lyellii
Pallaviciniales
Makinoa crispata
Fossombronia angulosa
Petalophyllum ralfsii
Fossombroniales
Pelliidae
Cryptomitrium tenerum
Mannia triandra
Asterella tenella
Plagiochasma wrightii
Reboulia hemisphaerica
Corsinia coriandrina
Cronisia fimbriata
Exormotheca bischleri
Oxymitra cristata
Riccia crustata
Riccia glauca
Riccia fluitans
Dumortiera hirsuta
Wiesnerella denudata
Targionia hypophylla
Clevea hyalina
Peltolepis quadrata
Sauteria alpina
Athalamia pinguis
Conocephalum conicum
Monoclea forsteri
Cyathodium tuberosum
Marchantia polymorpha
Preissia quadrata
Bucegia romanica
Marchantiales
Marchantiidae
Blasiidae
Neohodgsonia mirabilis
Neohodgsoniales
Riella parisii
Sphaerocarpos texanus
Monocarpus sphaerocarpus
Sphaerocarpales
Blasia pusilla
Blasiales
Apotreubia nana
Haplomitrium blumei
HAPLOMITRIOPSIDA
MARCHANTIOPSIDA

Extended Data Figure 5. Annotated ASTRAL phylogeny of liverworts inferred from amino acid data, highlighting suprafamilial relationships. Quartet values for the three possible topologies are presented as percentages near the node. Branches with maximum local posterior probability (lpp) are represented as solid black lines; those with a lpp between 0.8 and 1.0 as a solid grey line and those with a lpp below 0.80 as a grey dashed line; see Fig. S7 for detailed lpp for all branches. Asterisk marks novel order, and double Asterisk resurrected order.

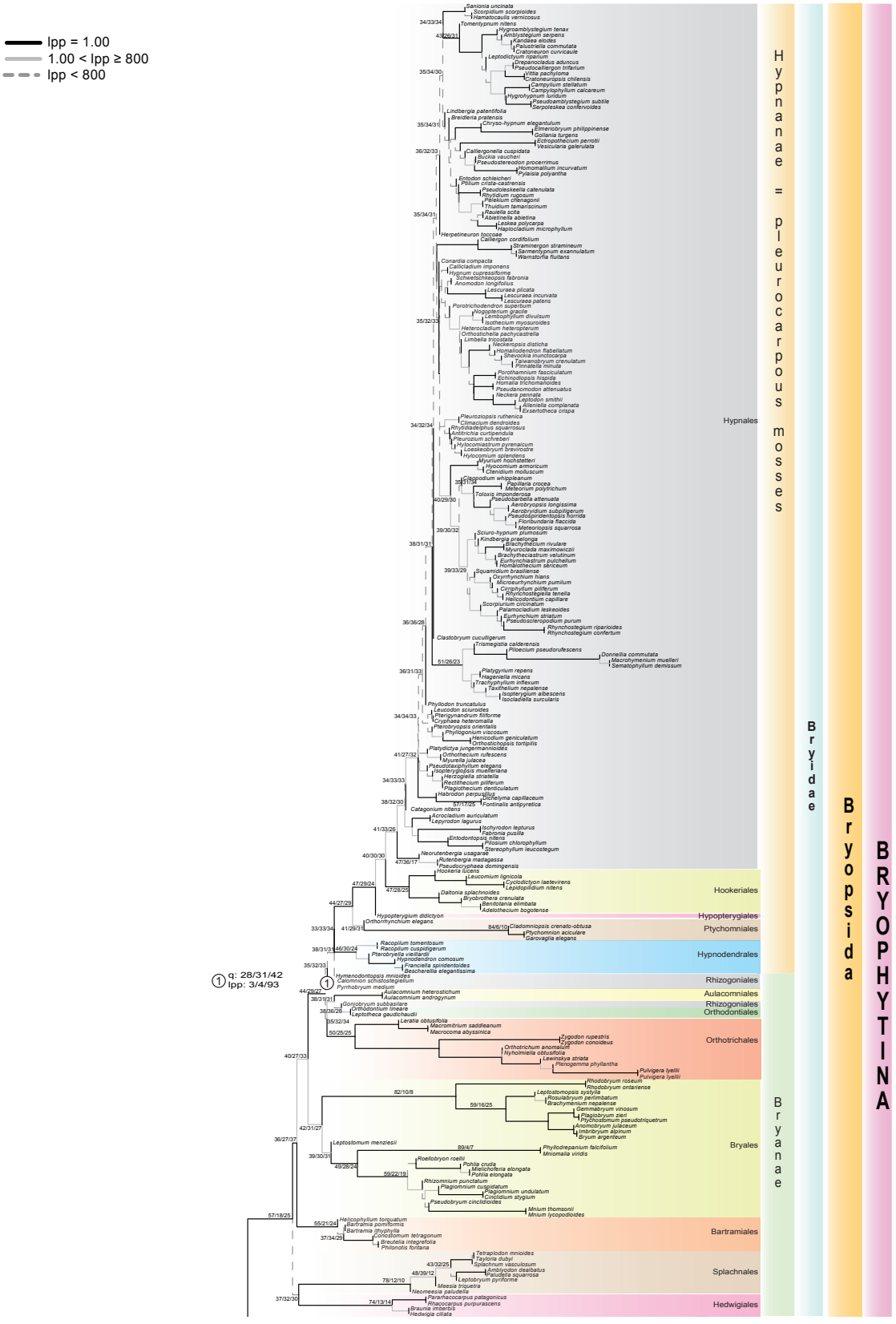
lpp = 1.00
1.00 < lpp ≥ 800
lpp < 800
q: 28/31/42
lpp: 3/4/93
Hypnanae = pleurocarpous mosses
Bryidae
Bryopsida
BRYOPHYTINA
Hypnales
Hookeriales
Hypopterygiales
Ptychomniales
Hypnodendrales
Rhizogoniales
Aulacomniales
Rhizogoniales
Orthodontiales
Orthotrichales
Bryales
Bartramiales
Splachnales
Hedwigiales
Bryanae

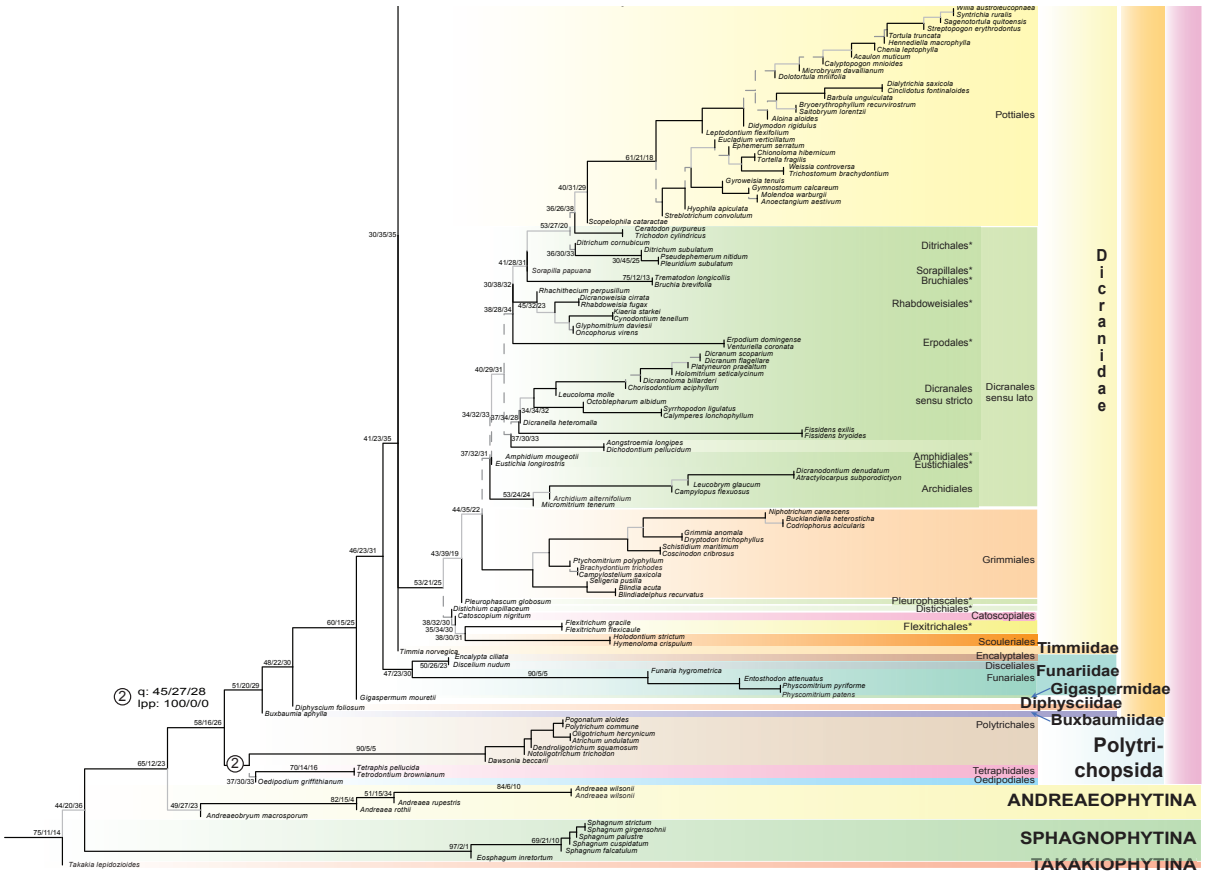

Extended Data Figure 6 Annotated ASTRAL phylogeny of mosses inferred from amino acid data, highlighting suprafamilial relationships. Quartet values for the three possible topologies are presented as percentages near selected nodes; see Fig. S6 for quartet values for all other branches. Branches with maximum local posterior probability (lpp) are represented as solid black lines; those with a lpp between 0.8 and 1.0 as a solid grey line and those with a lpp below 0.80 as a grey dashed line; see Fig. S7 for detailed lpp for all branches. Asterisks mark novel orders.

ED Fig. 7A

ED Fig. 7B

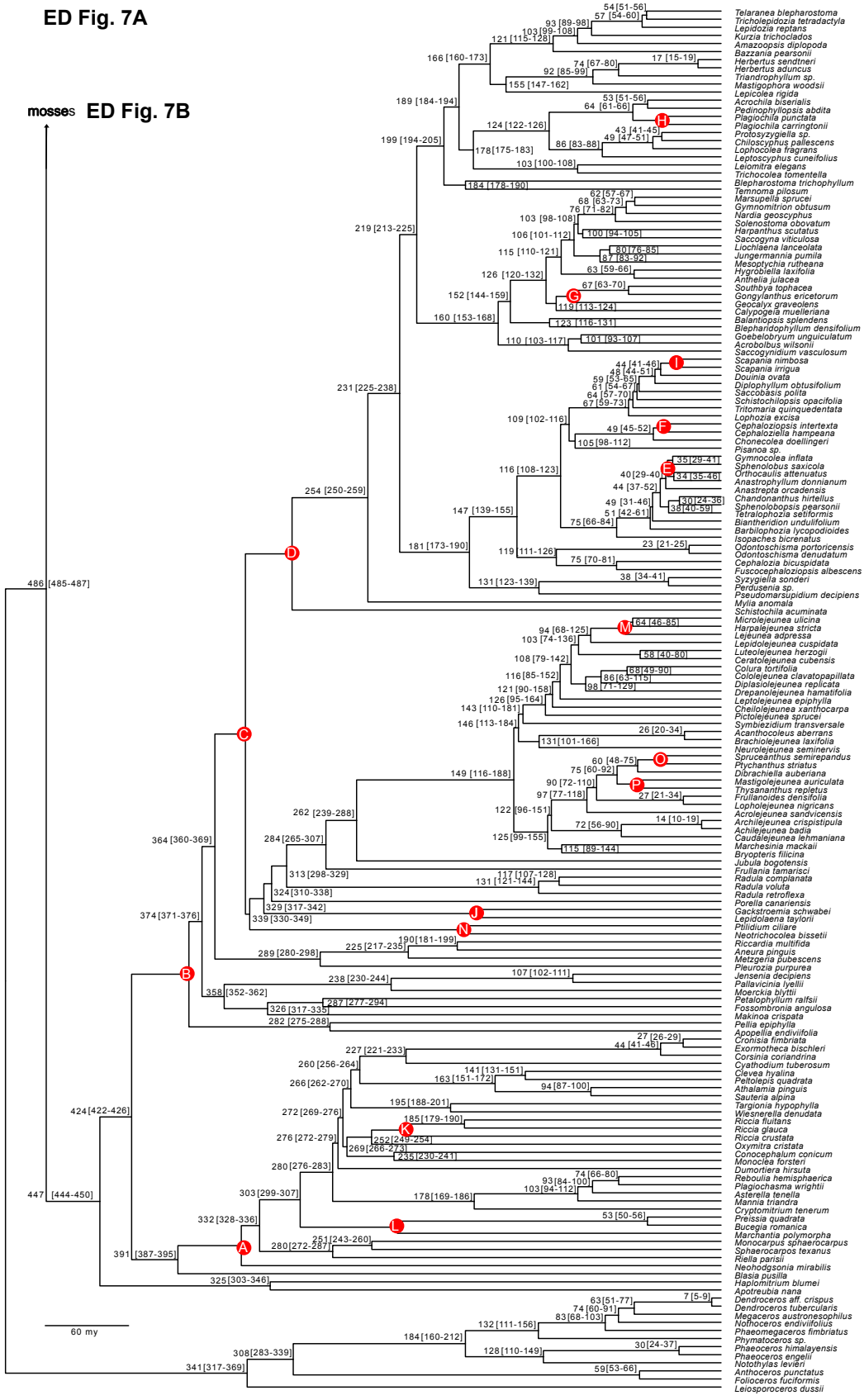

ED Fig. 7B

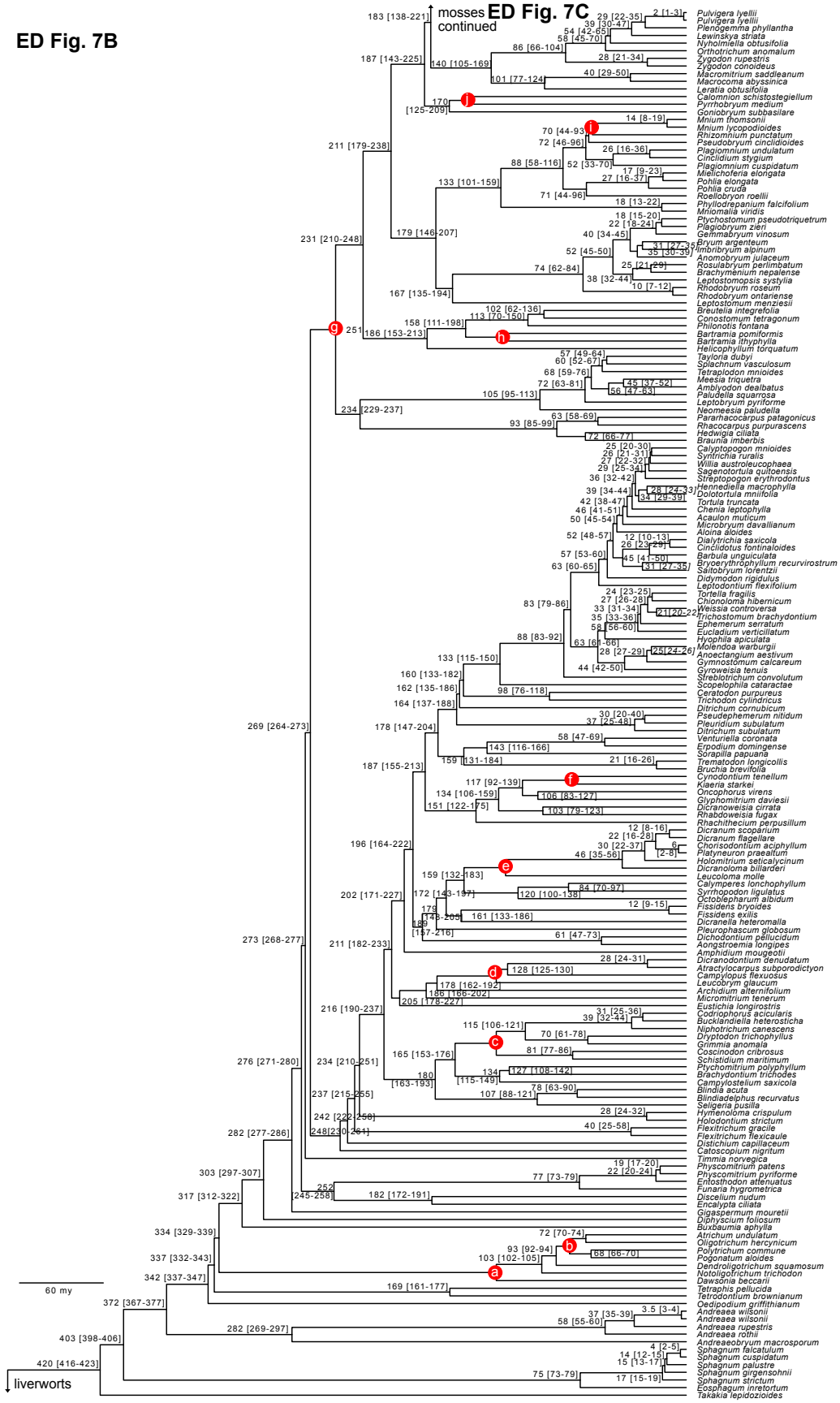
mosses continued
ED Fig. 7C
60 my
liverworts
Pulvigera lyellii
Plenogemma phyllantha
Lewinskya striata
Nyholmiella obtusifolia
Orthotrichum anomalum
Zygodon rupestris
Zygodon conoideus
Macromitrium saddleanum
Macrocoma abyssinica
Leratia obtusifolia
Calomnion schistostegiellum
Pyrrhobryum medium
Goniobryum subbasilare
Mnium thomsonii
Mnium lycopodioides
Rhizomnium punctatum
Pseudobryum cinclidioides
Plagiomnium undulatum
Cinclidium stygium
Plagiomnium cuspidatum
Mielichoferia elongata
Pohlia elongata
Pohlia cruda
Roellobryon roellii
Phyllodrepanium falcifolium
Mniomalia viridis
Ptychostomum pseudotriquetrum
Plagiobryum zieri
Gemmabryum vinosum
Bryum argenteum
Imbribryum alpinum
Anomobryum julaceum
Rosulabryum perlimbatum
Brachymenium nepalense
Leptostomopsis systylia
Rhodobryum roseum
Rhodobryum ontariense
Leptostomum menziesii
Bréutelia integrefolia
Conostomum tetragonum
Philonotis fontana
Bartramia pomiformis
Bartramia ithyphylla
Helicophyllum torquatum
Tayloria dubyi
Splachnum vasculosum
Tetraplodon mnioides
Meesia triquetra
Amblyodon dealbatus
Paludella squarrosa
Leptobryum pyriforme
Neomeesia paludella
Pararhacocarpus patagonicus
Rhacocarpus purpurascens
Hedwigia ciliata
Braunia imberbis
Calyptopogon mnioides
Syntrichia ruralis
Willia austroleucophaea
Sagenotortula quitoensis
Streptopogon erythrodontus
Hennediella macrophylla
Dolotortula mniifolia
Tortula truncata
Chenia leptophylla
Acaulon muticum
Microbryum davallianum
Aloina aloides
Dialytrichia saxicola
Cinclidotus fontinaloides
Barbula unguiculata
Bryoerythrophyllum recurvirostrum
Saitobryum lorentzii
Didymodon rigidulus
Leptodontium flexifolium
Tortella fragilis
Chionoloma hibernicum
Weissia controversa
Trichostomum brachydontium
Ephemerum serratum
Eucladium verticillatum
Hyophila apiculata
Molendoa warburgii
Anoectangium aestivum
Gymnostomum calcareum
Gyroweisia tenuis
Streblotrichum convolutum
Scopelophila cataractae
Ceratodon purpureus
Trichodon cylindricus
Ditrichum cornubicum
Pseudephemerum nitidum
Pleuridium subulatum
Ditrichum subulatum
Venturiella coronata
Erpodium domingense
Sorapilla papuana
Trematodon longicollis
Bruchia brevifolia
Cynodontium tenellum
Kiaeria starkei
Oncophorus virens
Glyphomitrium daviesii
Dicranoweisia cirrata
Rhabdoweisia fugax
Rhachithecium perpusillum
Dicranum scoparium
Dicranum flagellare
Chorisodontium aciphyllum
Platyneuron praealtum
Holomitrium seticalycinum
Dicranoloma billardieri
Leucoloma molle
Calymperes lonchophyllum
Syrrhopodon ligulatus
Octoblepharum albidum
Fissidens bryoides
Fissidens exilis
Dicranella heteromalla
Pleurophascum globosum
Dichodontium pellucidum
Aongstroemia longipes
Amphidium mougeotii
Dicranodontium denudatum
Atractylocarpus subporodictyon
Campylopus flexuosus
Leucobrym glaucum
Archidium alternifolium
Micromitrium tenerum
Eustichia longirostris
Codriophorus acicularis
Bucklandiella heterosticha
Niphotrichum canescens
Dryptodon trichophyllus
Grimmia anomala
Coscinodon cribrosus
Schistidium maritimum
Ptychomitrium polyphyllum
Brachydontium trichodes
Campylostelium saxicola
Blindia acuta
Blindiadelphus recurvatus
Seligeria pusilla
Hymenoloma crispulum
Holodontium strictum
Flexitrichum gracile
Flexitrichum flexicaule
Distichium capillaceum
Catoscopium nigritum
Timmia norvegica
Physcomitrium patens
Physcomitrium pyriforme
Enthostodon attenuatus
Funaria hygrometrica
Discelium nudum
Encalypta ciliata
Gigaspermum mouretii
Diphyscium foliosum
Buxbaumia aphylla
Atrichum undulatum
Oligotrichum hercynicum
Polytrichum commune
Pogonatum aloides
Dendroligotrichum squamosum
Notoligotrichum trichodon
Dawsonia beccarii
Tetraphis pellucida
Tetrodontium brownianum
Oedipodium griffithianum
Andreaea wilsonii
Andreaea wilsonii
Andreaea rupestris
Andreaea rothii
Andreaeobryum macrosporum
Sphagnum falcatulum
Sphagnum cuspidatum
Sphagnum palustre
Sphagnum girgensohnii
Sphagnum strictum
Eosphagum inretortum
Takakia lepidoziodes

ED Fig. 7C

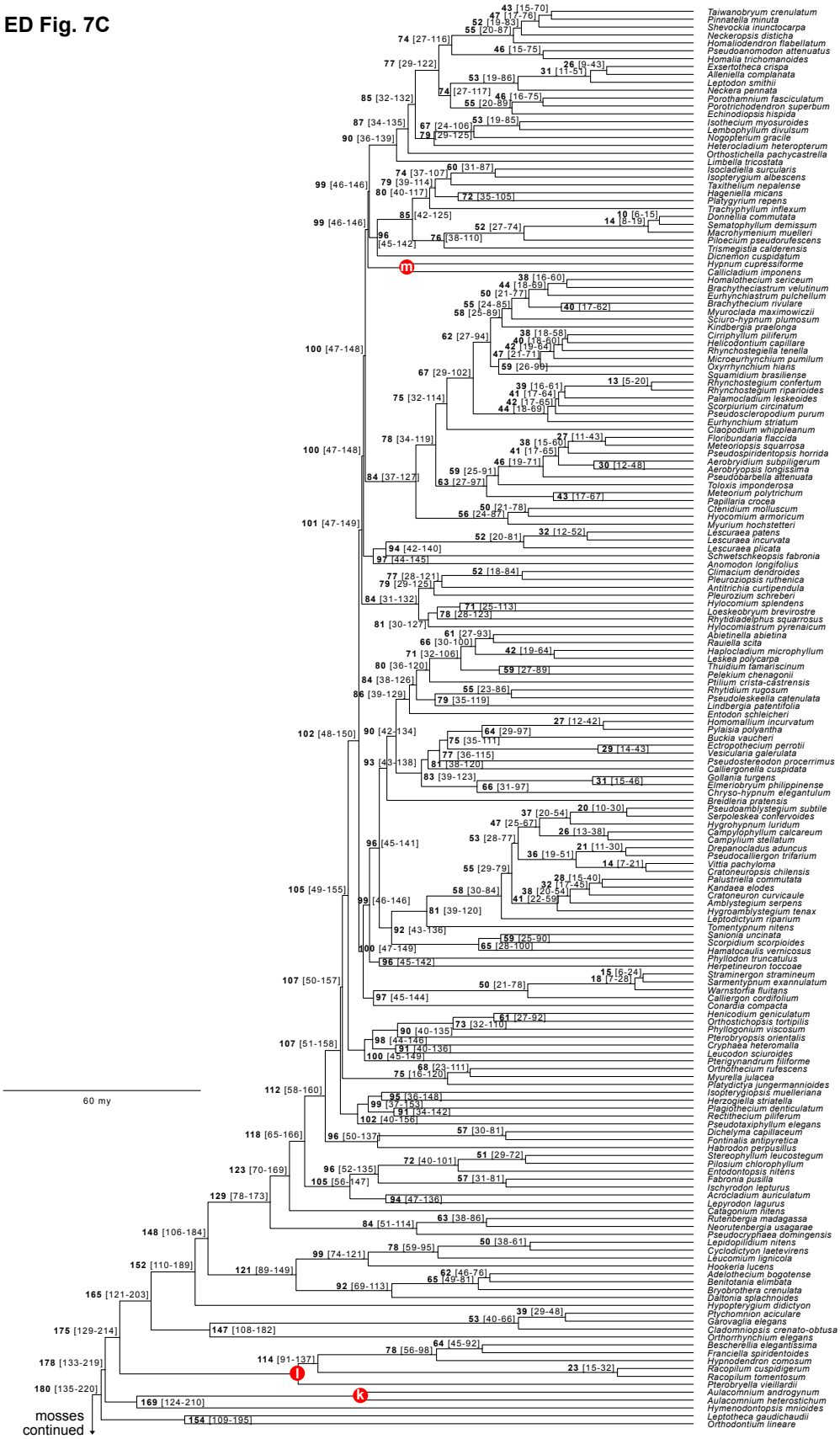
60 my
mosses continued ↓
Taiwanobryum crenulatum
Pinnatella minuta
Shevockia inunctocarpa
Neckeropsis disticha
Homaliodendron flabellatum
Pseudoanomodon attenuatus
Homalia trichomanoides
Exsertotheca crispa
Alleniella complanata
Leptodon smithii
Neckera pennata
Porothamnium fasciculatum
Porotrichodendron superbum
Echinodiopsis hispida
Isothecium myosuroides
Lembophyllum divulsum
Nogopterium gracile
Heterocladium heteropterum
Orthostichella pachycastrella
Limbella tricostata
Isocladiella surcularis
Isopterygium albescens
Taxithelium nepalense
Hageniella micans
Platygyrium repens
Trachyphyllum inflexum
Donnellia commutata
Sematophyllum demissum
Macrohymenium muelleri
Piloecium pseudorufescens
Trismegistia calderensis
Dicnemon cuspidatum
Hypnum cupressiforme
Callicladium imponens
Homalothecium sericeum
Brachytheciastrum velutinum
Eurhynchiastrum pulchellum
Brachythecium rivulare
Myuroclada maximowiczii
Sciuro-hypnum plumosum
Kindbergia praelonga
Cirriphyllum piliferum
Helicodontium capillare
Rhynchostegiella tenella
Microeurhynchium pumilum
Oxyrrhynchium hians
Squamidium brasiliense
Rhynchostegium confertum
Rhynchostegium riparioides
Palamocladium leskeoides
Scorpiurium circinatum
Pseudoscleropodium purum
Eurhynchium striatum
Claopodium whippleanum
Floribundaria flaccida
Meteoriopsis squarrosa
Pseudospiridentopsis horrida
Aerobryidium subpiligerum
Aerobryopsis longissima
Pseudobarbella attenuata
Toloxis imponderosa
Meteorium polytrichum
Papillaria crocea
Ctenidium molluscum
Hyocomium armoricum
Myurium hochstetteri
Lescuraea patens
Lescuraea incurvata
Lescuraea plicata
Schwetschkeopsis fabronia
Anomodon longifolius
Climacium dendroides
Pleuroziopsis ruthenica
Antitrichia curtipendula
Pleurozium schreberi
Hylocomium splendens
Loeskeobryum brevirostre
Rhytidiadelphus squarrosus
Hylocomiastrum pyrenaicum
Abietinella abietina
Rauiella scita
Haplocladium microphyllum
Leskea polycarpa
Thuidium tamariscinum
Pelekium chenagonii
Ptilium crista-castrensis
Rhytidium rugosum
Pseudoleskeella catenulata
Lindbergia patentifolia
Entodon schleicheri
Homomallium incurvatum
Pylaisia polyantha
Buckia vaucheri
Ectropothecium perrotii
Vesicularia galerulata
Pseudosteredon procerrimus
Calliergonella cuspidata
Gollania turgens
Elmeriobryum philippinense
Chryso-hypnum elegantulum
Breidleria pratensis
Pseudamblystegium subtile
Serpoleskea confervoides
Hygrohypnum luridum
Campylophyllum calcareum
Campylium stellatum
Drepanocladus aduncus
Pseudocalliergon trifarium
Vittia pachyloma
Cratoneuropsis chilensis
Palustriella commutata
Kandaea elodes
Cratoneuron curvicaule
Amblystegium serpens
Hygroamblystegium tenax
Leptodictyum riparium
Tomentypnum nitens
Sanionia uncinata
Scorpidium scorpioides
Hamatocaulis vernicosus
Phyllodon truncatulus
Herpetineuron toccoae
Straminergon stramineum
Sarmentypnum exannulatum
Warnstorfia fluitans
Calliergon cordifolium
Conardia compacta
Henicodium geniculatum
Orthostichopsis tortipilis
Phyllogonium viscosum
Pterobryopsis orientalis
Cryphaea heteromalla
Leucodon sciuroides
Pterigynandrum filiforme
Orthothecium rufescens
Myurella julacea
Platydictya jungermannioides
Isopterygiopsis muelleriana
Herzogiella striatella
Plagiothecium denticulatum
Rectithecium piliferum
Pseudotaxiphyllum elegans
Dichelyma capillaceum
Fontinalis antipyretica
Habrodon perpusillus
Stereophyllum leucostegum
Pilosium chlorophyllum
Entodontopsis nitens
Fabronia pusilla
Ischyrodon lepturus
Acrocladium auriculatum
Lepyrodon lagurus
Calagonium nitens
Rutenbergia madagassa
Neorutenbergia usagarae
Pseudocryphaea domingensis
Lepidopilidium nitens
Cyclodictyon laetevirens
Leucomium lignicola
Hookeria lucens
Adelothecium bogotense
Benitotania elimbata
Bryobrothera crenulata
Daltonia splachnoides
Hypopterygium didictyon
Ptychomnion aciculare
Garovaglia elegans
Cladomniopsis crenato-obtusa
Orthorrhynchium elegans
Bescherellia elegantissima
Franciella spiridentoides
Hypnodendron comosum
Racopilum cuspidigerum
Racopilum tomentosum
Pterobryella vieillardii
Aulacomnium androgynum
Aulacomnium heterostichum
Hymenodontopsis mnioides
Leptotheca gaudichaudii
Orthodontium lineare

Extended Data Figure 7. Divergence times estimates for bryophytes inferred by penalized likelihood using 29 fossil calibrations. Mean node ages (in bold) including confidence intervals (in brackets) reported in millions of years are stemming from a treePL analysis. Letters in red circles indicate fossil calibrations as outlined in Table S2. The figure is divided in three parts: liverworts and hornworts: Extended Data Figure 7A, mosses Extended Data Figures 7B & C.

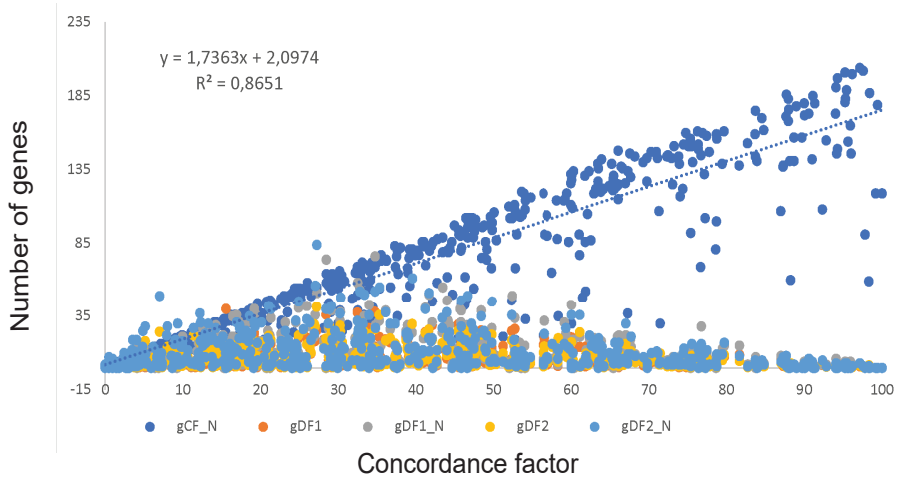

Extended Data Figure 8. Correlation between gene concordance factor inferred by IQ-TREE and number of genes in the nucleotide dataset supporting a node. For details on the concordance values see Table S5

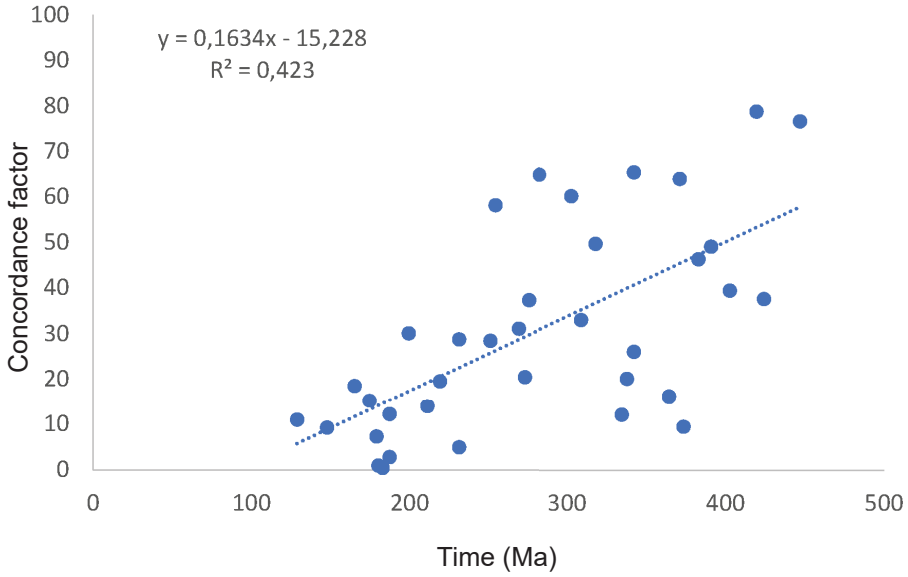

Extended Data Figure 9. Correlation between gene concordance factor inferred by IQ-TREE and mean divergence times for backbone nodes (between 130-450 Ma) inferred from the nucleotide data. For details on the concordance values see Table S5.

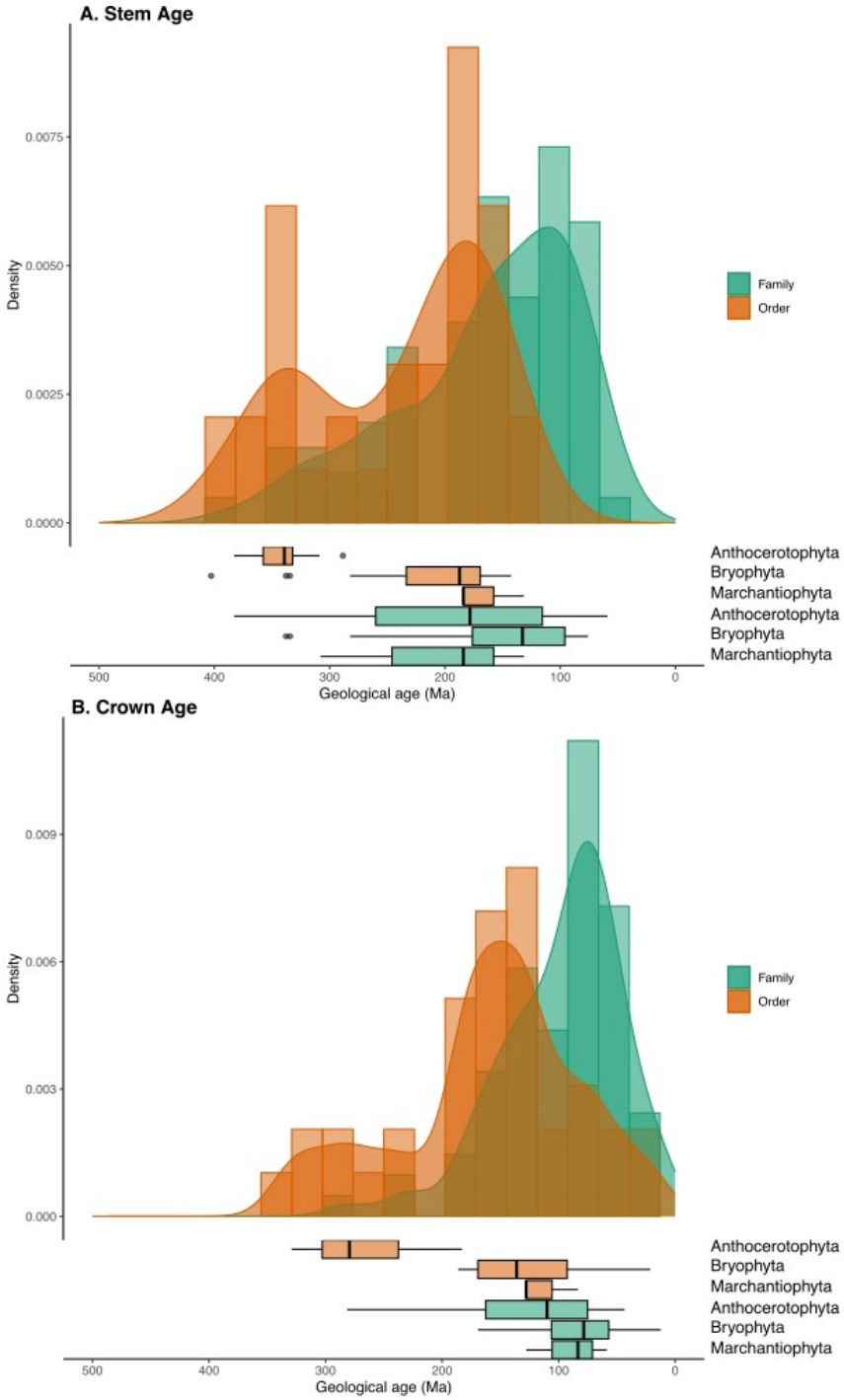

Extended Data Figure 10. Histogram of the frequency of orders and families (A) stem and (B) crown estimated age divergences of three bryophyte phyla (Anthocerotophyta, Bryophyta, and Marchantiophyta). Kernel density plots depict the probability distribution (95% confidence interval) of the estimated divergence time of orders and families. Boxplots at the bottom show the distribution of the estimated age divergences of orders and families separated for Anthocerotophyta, Bryophyte, and Marchantiophyta.